NTNU – Trondheim
Norwegian University of
Science and Technology

Broadband processing of conventional 3D seismic data for near surface geohazard investigation: A North Sea case study

Arv Håkon Breistøl

Petroleum Geoscience and Engineering
Submission date: June 2015
Supervisor: Martin Landrø, IPT
Co-supervisor: Vetle Vinje, CGG

Norwegian University of Science and Technology
Department of Petroleum Engineering and Applied Geophysics

Preface

The following master's thesis in Petroleum Geophysics was submitted to the Department of Petroleum Engineering and Applied Geophysics at the Norwegian University of Science and Technology (NTNU) 10. June 2015. The project was supervised by professor Martin Landrø and was executed in collaboration with CGG Services (Norway) AS. The work is a part of the LOSEM project, a research consortium comprising founding sponsors CGG, BayernGas, Lundin Petroleum, Statoil and Total.

The content of the following master's thesis propose a cost effective input to the de-risking of offshore E&P prospects by utilizing 3D seismic exploration data in a geo-hazard assessment. At time of submission companies all over the oil & gas industry are announcing short- and long-term cost cuts to maintain profitable operation in the reduced oil price environment. At the same time, human and environmental safety is still held at top priority in the planning and development of the operation. These two factors combined effectively call for innovative resource management. The aim of this master's thesis is to describe a processing workflow that prepares acquired exploration data for a defined geohazard assessment through targeted processing. The workflow is preformed at a North Sea data set, acquired in 1991 over an underground blowout, where the primary goal was to identify an efficient workflow that assessed the main challenges in the acquired data while preserving the resolution in a reliable way.

I would like to acknowledge Thomas Elboth, Erik Hicks, Jamshade Khan, Carl-Inge Colombo Nilsen, Vetle Vinje, Terje Weisser, and my supervisor Martin Landrø, all for their utmost help and support in this thesis. Further, a special thanks to LOSEM founding sponsors BayernGas, Lundin Petroleum, Statoil, Total, and CGG for their financial investments and academic interest in my research.

Norway, June 2015 Arv Håkon Breistøl

Abstract

3D exploration seismic data is increasingly being utilized for geohazard studies in the offshore oil and gas industry. An important criterion for the success of this approach is that the seismic data contain the broadest frequency bandwith possible. This study aims to display the potential of old vintage 3D exploration data in geohazard studies using targeted broadband processing.

The processing workflow delivers a near surface volume suitable for geohazard assessment. A Central North Sea data set, acquired in 1991 by Geco-Prakla using a dual source/dual streamer-configuration, was processed using best practice commercial processing technology to image a shallow gas hazard.

Raw shot gathers displayed decent quality, but suffered from seismic ghosts, low frequent linear noise trends and multiples. The data was source designatured using a custom signature deconvolution successfully recovering frequencies in 80-100 Hz range. A K-filter followed by a Radon filter was applied, effectively mitigating the main linear noise content. Receiver deghosting was performed using least squares linear Radon equations showing enhanced imaging, but limited improvement in the frequency spectrum arguably due to natural notch diversity in the acquisition stage. Demultiple was performed using tau-p gap deconvolution, before binning and regularization was applied. Migration was done using pre-stack Kirchhoff time algorithm with 3000 m migration aperture, 4700 m maximum travel time aperture, and an anti-alias filter. The workflow imaged clear amplitude anomalies around the well trajectory at 520 ms and 650 ms two way traveltime depth.

The work demonstrates the use of conventional 3D seismic exploration data in a shallow gas geohazard study. Using targeted processing we were able to define the extent and magnitude of the shallow gas hazard, effectively illustrating its value and potential in proactive risk assessment for the offshore hydrocarbon exploration and production.

Sammendrag

3D seismikk fra leteoperasjoner blir i økende grad anvendt i studier av geofarer for den marine olje- og gassindustrien. Et viktig kriterium for suksessfull anvendelse er at de seismiske dataene inneholder det bredeste frekvensbåndvidden som mulig. Denne oppgaven ønsker å vise potensialet til gammel 3D letedata i studier av geofarer ved hjelp av målrettet bredbåndsprosessering.

Den foreslåtte arbeidsflyten produserer et seismikkvolum for evaluering av marine geofarer. Et Nordsjø-datasett, innsamlet i 1991 av Geco-Prakla med en to-kilde/to-kabel-konfigurasjon, ble prosessert ved hjelp av kommersiell prosesseringsteknologi med hensikt å avbilde en grunn gassfare.

Rå skuddsamlinger antydet data av god kvalitet, men inneholdt tydelige seismiske spøkelser, lavfrekvent lineær støy og multipler. Dataene ble kilde-avsignert ved hjelp av en skreddersydd signaturdekonvolusjon som suksessfullt gjenskapte signaler i frekvensområdet 80-100 Hz. Et K-filter etterfulgt av Radon-filter ble anvendt for å effektivt fjerne mesteparten av det lineære støyinnholdet. Mottakeravspøkning ved hjelp av minste kvadraters lineære Radon-ligninger viste forbedret avbildning, mens begrensede forbedringer i frekvensinnhold trolig skyldes naturlig diversivitet i spøkelseshakkene fra innsamlingsstadiet. Migrasjon ble utført med pre-stakk Kirchhoff's tidsalgoritme med 3000 m apertur, 4700 m maksimum gangtid apertur og et antialias-filter. Arbeidsflyten avbildet klare amplitudeanomalier rundt den tidligere brønnbanen på 520 ms og 650 ms toveis gangtid dyp.

Studiet demonstrerer effektivt bruken av konvensjonell 3D seismikk i et grunt gass-geofare-studie. Ved hjelp av målrettet prosessering er det mulig å definere utvidelse og omfang til den grunne gassfaren, som tydelig illustrerer den potensielle verdien til selv utdatert letedata i proaktiv riskikostyring for den marine olje- og gassnæringen.

Contents

List of Figures

Chapter 1

Introduction

In the hydrocarbon production, a geohazard is any geological phenomenon or process that may pose a safety risk to the crew, the installation, the environment or the operation (Campbell, 2003). Offshore shallow geohazards are considered by evaluating the seabed and the rock volume down to 1 ms two-way time below the seabed. In the last decades offshore geohazards have become highly relevant with the increasing attention divided to human and environmental safety. A large number of major oil companies currently list the reduction of geohazard related risks among their top research priorities (Solheim et al., 2005).

The marine engineering geophysicist's role in a geohazard assessment is to apply appropriate geophysical tools and utilize data to assess relevant parameters in a quantitative manner. Conventional site survey technology, including sonar and sub-bottom profilers, yield high resolution data but are expensive and demand additional acquisition. Conventional 3D exploration seismic data is currently experiencing increased attention in geohazard assessments by the oil & gas industry (Farouki and Sakamoto, 2013). Seismic streamer data is by industry standard main data input to the exploration campaigns, utilizing the seismic depth image and estimated parameters such as pore pressure fracture gradients and geomechanical properties to plan the well. Economical and logistical rationality therefore suggest that utilizing the already acquired seismic data for the geohazard assessment would be an cost-effective approach to resource management. However, narrow bandwidth has historically restrained the resolution, limiting the use of conventional exploration seismic data in the geohazard assessments.

In marine seismic context the ghost refers to upgoing energy reflected at the water surface superimposing the primary energy of interest, leading to constructive and destructive interferences in the wavefield (Sheriff and Geldart, 1995, p. 163). The ghost effectively limits the frequency content and thus constrains the imaging resolution, and has for these reasons been considered as a major threat to data integrity ever since the very beginning of reflection seismology (Amundsen and Landrø, 2013b). Innovative research aiming to reduce the ghost's impact on the seismic data has the last years proved successful,

developing a wide range of deghosting techniques applicable for design of both acquisition instruments and processing algorithms.

The introduction of broadband seismic in the oil & gas industry has greatly improved the application of seismic data in geohazard assessments. Broadband acquisition is currently provided by all the large seismic contractors. A processing based broadband solution in geohazard assessments is however arguably more cost effective. It does not require additional acquisition effort, and the solution can be applied to the complete existing legacy data library acquired with conventional technology.

The content of the following master's thesis propose a cost effective input to the risking of offshore E&P prospects by utilizing 3D seismic exploration data in a geohazard assessment. The work seek to explore the challenges in conventional seismic data that may be assessed in processing stage by targeting a known shallow gas geohazard in the Central North Sea. In 1989 the study area experienced a major underground blow out lasting for 326 days (Landrø, 2011). Remen (1991) estimates 0.4 million m^3 of oil and 196-367 million m^3 of gas migrated from the reservoir into shallow formations before the blow out was killed using a relief well. Main recipients for the hydrocarbons are suggested to be thin sand layers at approximately 490 m and 840 m below mean sea level. By using best practice commercial processing technology this broadband processing work flow will specifically target these shallow gas recipients to open up for new quantitative 3D studies of the area.

Ch. 2 serves as an introduction to the basics of seismology, conventional reflection seismic and commercial acquisition, before a discussion of the seismic ghost and its implications on the resolution is given. Further, the broadband industry solutions are discussed followed by a theoretical introduction to seismic processing, before presenting broadband processing as a concept. Ch. 3 targets the offshore shallow geohazards by defining the term and presenting the implications of proactive geohazard assessment. It further presents three important geohazards to display the range of considerations relevant for a shallow geohazard study. The chapter continues by briefly discussing geohazards on the Norwegian continental shelf, before reviewing the conventional site survey technology utilized in industry geohazard assessments. Finally the use of seismic data in geohazard evaluations are discussed and compared with the site survey technology, emphezising the use and limitation of conventional seismic data. Ch. 4 is dedicated to the processing of the North Sea case study. It introduces the dataset and discuss the complete applied work flow in greater detail. Ch. 5 discuss the results and the challenges. In Ch. 6 concluding remarks are given, before recommendation for further work and research is stated in Ch. 7.

Chapter 2

Seismic acquisition and data processing

2.1 Seismic reflection data

Reflection seismology is widely recognized as the most important concept applied for subsurface investigation within the oil and gas industry. The fundamentals of seismic exploration are based on letting a controlled source generate seismic energy before measuring the time required for the seismic waves to propagate to a series of recorders at given datums, through the media of interest. A main geophysical objective of seismic exploration is hence to attempt to reconstruct the paths of the seismic waves and derive accurate information about the subsurface media based on these arrival times and the recorded variations in amplitude, frequencies and waveforms (Sheriff and Geldart, 1995, p. 1).

Partitioning of propagating wave energy at interfaces is the elementary occurrence of seismology, being the prerequisite for the recorded reflections. The Zoeppritz equations (Zoeppritz, 1919) present predictions of how both pressure and shear energy can be reflected and transmitted at an interface, based on boundary conditions or layer parameters. As derived by Sheriff and Geldart (1995) among others, these equations can again be simplified for a normal incidence pressure wave at a single, horizontal boundary, as illustrated in **Fig. 2.1**. Here v_{pn} is the P-wave velocity of layer n and ρ_n is the bulk density of layer n, while α_I , α_T and α_R denotes the displacement amplitudes for incidence ray, the transmitted ray and the reflected ray respectively.

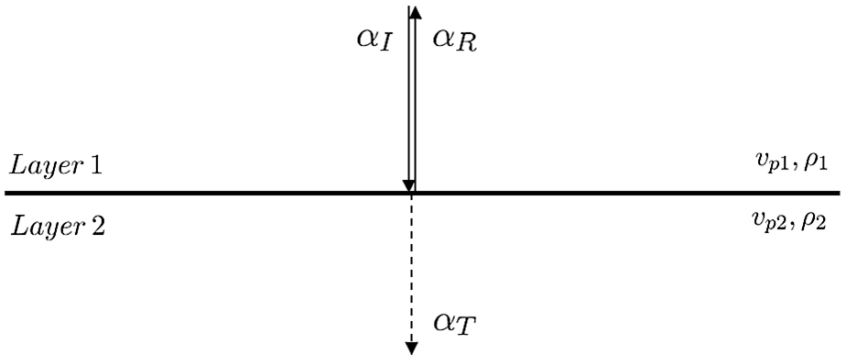

Figure 2.1 – *Normal incidence pressure wave at horizontal boundary, accompanied by its consequal reflected wave and transmitted wave*

Introducing the product of density and velocity for layer n as acoustic impedance, often denoted Z_n, Zoepporitz' equations can be reduced to simply stating

$$\alpha_I = \alpha_R + \alpha_T \tag{2.1}$$

$$-Z_1\alpha_I = Z_1\alpha_R + Z_2\alpha_T \tag{2.2}$$

that easily arrange into the widely known equations for zero-incidence reflection and transmission coefficients

$$R = \frac{\alpha_R}{\alpha_I} = \frac{v_{p2}\rho_2 - v_{p1}\rho_1}{v_{p2}\rho_2 + v_{p1}\rho_1} = \frac{Z_2 - Z_1}{Z_2 + Z_1} \tag{2.3}$$

and

$$T = \frac{\alpha_T}{\alpha_I} = 1 - R = \frac{2\rho_1 v_1}{v_1\rho_1 + v_2\rho_2} = \frac{2Z_1}{Z_1 + Z_2} \tag{2.4}$$

The important relation between a recorded wave field and the physical properties of the reflective layers needs to be established in geological terms before being interpreted and used in reservoir characterization. As the media of interest in subsurface imaging is geological facies, changes in the acoustic impedances are often assumed to represent relevant geological boundaries. As a result, structural interpretation of seismic data analysis is primarily based on identifying traveltimes that are coincident with geological layer boundaries, while stratigraphic interpretation is often based on manipulation of seismic amplitudes to enhance subtle features associated with depositional environment and sedimentology (Yilmaz, 2001, Ch. 7.5).

For reservoir characterization beyond reflection interpretation we may apply more advanced concepts, usually requiring association of rock physics models, field data or statistical algorithms with our seismic records. Seismic inversion serves to extract quantitative rock properties from the reflection series correlated with well logs or laboratory data. AVO-analysis, or amplitude variations with offset-analysis, seeks to establish subsurface parameters by analyzing seismic amplitudes as a function of reflection angle, using modelling of Zoeppritz equations. Both concepts may allow lithology characterization, porosity estimation and even fluid type discrimination from the seismic reflection data if applied successfully, but the techniques have many potential pitfalls and requires great caution (Avseth et al., 2005, Ch. 4.3).

There might be many geological and geophysical explanations for an amplitude reading in a recorded seismic trace, and not all of them are necessarily relevant for seismic interpretation and characterization (Hesthammer et al., 2001). Assuming that the wave field of interest is the primary reflection series from the subsurface, Sheriff (2002) defined seismic noise as all recorded energy other than primary reflection energy, claiming acquired seismic data in general contains a combination of the primary reflected signals and the accompanying seismic noise. The result is noise interfering with the primary reflection readings, jeopardizing structural and stratigraphic interpretation as the systematic noise features will limit the ability to distinguish non-geological artifacts from real features (Elboth and Hermansen, 2009).

And as stated by Hesthammer et al. (2001), the seismic data alone do not necessarily allow perfectly distinguishing of noise artifacts from real geological features. Hence should all seismic data be approached with caution, well aware that the key to successful interpretation and characterization lies in high quality data and careful assessment that recognizes both the geological and the geophysical aspects of the seismic.

2.2 Seismic resolution and frequency content

An important objective in interpretation of seismic data is to identify reservoir boundaries, and evaluate dimensions and geometries of exploration targets accurately from reflection configurations in the seismic section. In order to perform the interpretation as precise as possible, we seek to optimize the seismic resolution, the ability to distinguish separate features in the seismic data.

As discussed by Kallweit and Wood (1982) among others, the vertical resolving power can be considered by imaging a geological bed as it thins out, and evaluate the separation of the resulting readings on a recorded trace. A bed of sufficient thickness will produce individual, completely separated reflected wavelets from each of the two bounding interfaces, and the trace can in order potentially yield maximum possible information for each of the interfaces. Reyleigh's Criterion states that as the bed thickness diminishes and approaches one quarter of the dominant wavelength in the seismic wavefield, $\frac{\lambda}{4}$,

the energy becomes a composite of the two reflections, as illustrated in **Fig. 2.2**. The result is constructive interference between the wavelets, causing an amplitude increase often referred to as tuning, and the bed boundaries are no longer fully resolved. As the wavelength directly corresponds to frequency f and velocity v by $\lambda = \frac{v}{f}$ the well-known relation between the frequencies and the seismic resolution is established.

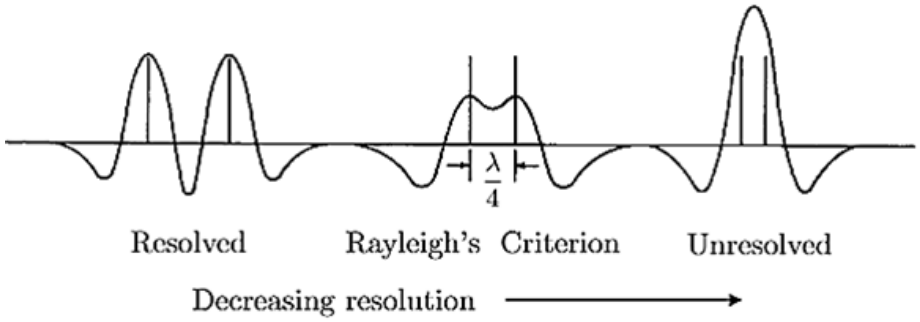

Figure 2.2 – *Reyleigh's Criterion. When two reflective features, e.g two positive acoustic impedance changes (illustrated by the vertical lines) are sufficiently separated, the two corresponding reflected wavelets are resolved. As the distance between the two acoustic impedance changes decreases, and meets $\frac{\lambda}{4}$, tuning occurs and the wavelets are no longer fully resolved. (Figure modified after Kallweit and Wood (1982))*

It can be shown that the amplitude of a spherical wave, such as the one produced from a point source, is inversely proportional to the distance travelled due to the elastic energy absorbed by the medium. To review this relative energy loss due to the elastic absorption per cycle of wave propagation we introduce the quality factor Q. Absorption can then be formulated as the relation between an initial amplitude A_0 and amplitude A recorded after time t as

$$A = A_0 e^{\frac{-\pi f t}{Q}}, \tag{2.5}$$

where Q is quality factor and f is the frequency. As Q itself is assumed frequency independent in the seismic frequency bandwidth, and frequency and wavelength are inversely proportional to each other, Eq. 2.5 implicates that absorption will be larger for the high frequencies having short wavelength, than for the low frequencies having long wavelength, as the latter will have fewer wave cycles per distance unit travelled. This effectively implies that low frequency seismic energy can propagate, and hence image, deeper compared with higher frequency energy. This is an important consideration especially for exploration and interpretation in highly absorbing lithological conditions, including sub-salt and sub-basalt plays. Presence of such litholgies disturbs the imaging and might conceal important underlying targets for interpretational purposes.

For the interpreter, the shape of the wavelet itself plays an important part, as sharp peaks allows more precise identification of amplitudes. The optimal wavelet for interpretation is

symmetrically shaped with dominant wave loop that corresponds to the actual reflection interface of the acoustic boundary, a so called symmetrical zero-phased wavelet. The concept of polarity indicates if the dominant loop is a peak or trough when passing a defined acoustic impedance boundary, and Society of Exploration Geophysicist defines the polarity convention for an increase in acoustic impedance as positive, displayed as a peak (Simm and White, 2002). It is established that the low frequencies play an important role in the shaping of the wavelet (Amundsen and Landrø, 2013a), as illustrated in **Fig. 2.3**. When keeping the high frequencies fixed and increasing the low frequencies, one can observe that the side lobes of the wavelet are reduced. This also increases the resolution of the data as these side lobes will be less likely to hide other reflection that coincides with them. When keeping low frequencies fixed and increasing the high frequencies, main peak is sharpened.

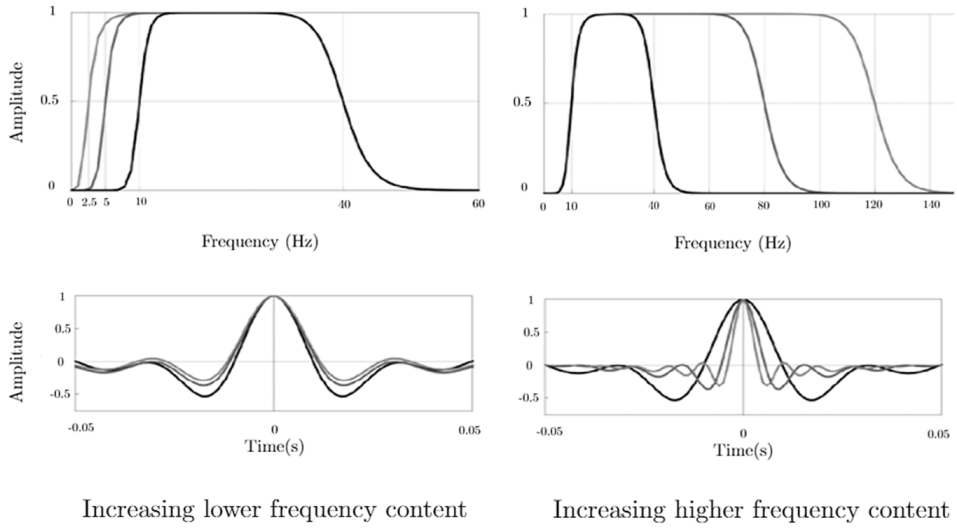

Figure 2.3 – *Temporal resolution frequency dependency. Left: Increasing the low frequency content corresponing to the brighter colours. Right: Increasing high frequency content corresponding to brighter colours. Source: Amundsen and Landrø (2013a)*

When assessing seismic data we hence seek to optimize the resolution, by preserving a frequency band ideally containing both high and low frequencies, in order to observe the data in highest resolution possible for accurate interpretation. (Sheriff and Geldart, 1995, p. 186)

2.3 Marine streamer acquisition

Production of offshore hydrocarbons started in the early 1940s and is today representing approximately $\frac{1}{3}$ of world crude oil production. Giant offshore fields, comprising 500 million bbl or more recoverable, accounts for 41 % of total oil discovered (Oil & Gas

Journal, 2007), and great effort and resources is, and has been, put into technological research of mechanical, geological, geophysical and computational engineering to improve efficiency and quality in offshore oil and gas industry. For subsurface investigation, the most important technique used in modern commercial offshore hydrocarbon exploration is the seismic marine streamer acquisition, as illustrated in **Fig. 2.4**. A vessel tows a seismic source, along with kilometer long cables equipped with seismic sensors, while paravanes are used to maintain correct relative positions between the equipment in the water. The acquisition is performed by moving the vessel and emitting energy from the source in a continuous manner while constantly recording the reflected energy from the subsurface, to effectively cover large areas, up to many thousand square kilometers, in a single survey.

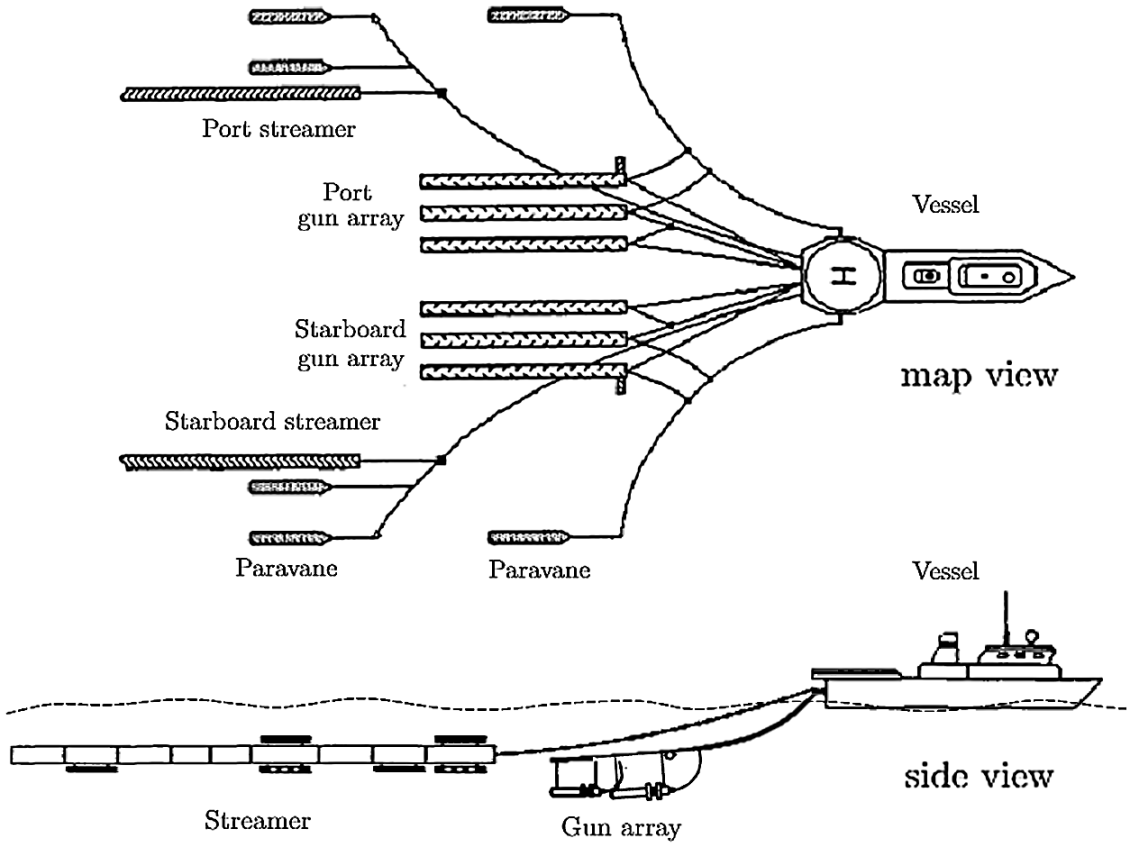

Figure 2.4 – *Marine streamer acquisition example in map view and side view. The seismic vessel tows a seismic source, typically an air gun array, along with seismic streamers. Paravanes are used to keep correct separation between the two gun arrays and the two cables. Illustration not to scale.*

The most common seismic source type in marine hydrocarbon exploration is the submerged air-gun array. It emerged in the industry in the 1970s, and has since then been the most popular seismic source due to its ease of use and deployment, predictability,

repeatability and reliability. An individual air-gun releases compressed air rapidly into the surrounding water to create an acoustic pulse of energy that can propagate through the water layer and into the media of interest. As the compressed air is released into the water, an oscillating bubble forms that will expand and collapse repeatedly on its way to the surface. A single expansion of the bubble would have resulted in an ideal, primary signal only, but the oscillating motion introduces undesirable cyclic bubble characteristics in the signature. Clustering of the air-guns with different volumes will, however, effectively improve the primary to bubble signal ratio and enhance the signal characteristics. A typical air-gun array can therefore consist of 3 - 6 sub-arrays called strings, fixed at between 3m and 10m below the sea surface, with each string containing 6 - 8 individual guns. This yields between 18 and 48 guns, firing at between every 10-15 seconds depending on the acquisition configuration and survey objective (Amundsen and Landrø, 2010a).

In marine seismic acquisition sensors and cables form a streamer towed by the seismic vessel. The sensors, called receivers or hydrophones, are pressure sensitive and uses piezoelectric transducers to create analogue signals. The streamer itself is a polyurethane tube, with diameter of 5-6 cm, filled with either fluid or solid foam for buoyancy. With length of up to tens of kilometers, each streamer is typically is made of 12-station, 150 m sections, with each station including 8-16 hydrophones and one analog-to-digital converter, routing the analogue signals to a digital seismic recorder in the vessel. (Meunier, 2011, Ch. 3) In conventional marine acquisition the streamer is deployed with a head and tail buoy, and is towed flat after the boat at a fixed depth, typically between 5-10 m depending on the objective of the survey. While some targeted operations still favour single streamer survey configuration, modern streamer and vessel technology now allows towing of up to 20-25 cables to improve efficiency in large scale surveys such as multi-client data acquisition.

Marine seismic acquisition introduces a set of distinct noise characteristics in the records that must be considered when assessing the seismic data. The noise might be either coherent or incoherent, and may originate from a wide range of sources depending on many different parameters, including character and condition of the vessel and its equipment, acquisition geometry, weather during operation and local sea level. When reviewing acquired data, an observers log or acquisition report provided by the contractor will describe in detail many of the important parameters and allow for better understanding of the nature of the noise to be expected in the data. Although varying from survey to survey, Elboth and Hermansen (2009) identified and discussed some of the most important types of noise present in a marine seismic survey acquired offshore; swell noise, hydrostatic pressure variation noise, tugging, cavitation noise and seismic interference.

The swell noise is high amplitude noise created by two different mechanisms. On fluid filled streamer the streamer motion can induce transverse waves internally generating swell noise up to around 10 Hz, but as most modern streamers now are foam filled, this noise is rarely seen in modern seismic data. Swell noise can also be caused by cross flow over the streamer, induced by ocean currents. Unsteady flow creating vortexes produces

strong alternating pressure fluctuations that will be observed as high-amplitude swell-noise in the seismic records on both old and modern streamer data.

Hydrostatic pressure variation relates directly to the height of the water column over the seismic streamer, and is caused by streamer buckling and ocean swells. The frequency content of hydrostatic pressure variations is however limited to typically 0-2 Hz, a frequency band not normally containing much useful seismic data.

Tugging noise is caused by sudden movements of the vessel due to wave motion, and is typically most prominent on the first sections on a streamer. The tug noise increase proportional with angle between head and tail buoy, suggesting that tug noise increase when towing deeper. In addition to tugging, vibrations or strumming from the lead-in cables also affect some seismic gathers. This kind of noise is characterized by relatively large amplitudes in a narrow frequency band typically between 3-10 Hz.

Cavitation noise from the propeller as it moves through the water is one of several noise types originating from the operating vessel. As low pressure volumes form as the fluid accelerates and moves past blades, fluids undergo phase transition into vapor and form small bubbles that collapse and cause strong local cavitation waves seen as periodic noise in seismic data. Amundsen and Landrø (2011) suggest that rapid movement of air escaping through air-gun ports creates cavities that also could be a potential source of high frequency noise affecting the recorded data.

Seismic interference from other vessel activity is also visible in the seismic sections. The interference is often broad banded in the frequency spectra and can have large amplitudes compared to subsurface reflection data. Information on other ongoing acquisition is often mentioned specifically in the observers logs or acquisition reports along with accurate information of sail line and shot numbers that is affected.

2.4 The ghost effect

The ghost was acknowledged in seismology already in the 1930s by Leet (1937) who observed that the initial kick in an onshore seismic velocity well reappeared 180 degrees out of phase after a time interval of less than twice the uphole time. Since then, countless articles has adressed the challenges related to the ghost and its impact on seismic reflection data. In *Encyclopedic Dictionary Of Applied Geophysics* Sheriff (2002) defines:

> **ghost: 1.** Energy that travels upward from an energy release and then is reflected downward, such as occurs at the base of the weathering or at the surface. Ghost energy usually joins with the down-traveling wave train to change the effective wave shape. Some times called **secondary reflection** (which is also applied to other multiples). **2.** Energy reflected from the water surface before being picked up by a submerged receiver.

The ghost is an unwanted, yet inevitable, phenomenon in marine seismic that concerns up-going energy reflecting at the water surface, both on source and receiver side of conventional streamer acquisition, as illustrated in **Fig. 2.5**. When the up-going pressure wave field meets the free surface between water and air, the large acoustic impedance contrast yields a strong, negative reflection guiding the energy down with a reversed polarity, where it constructively and destructively interferes with the primary wave field.

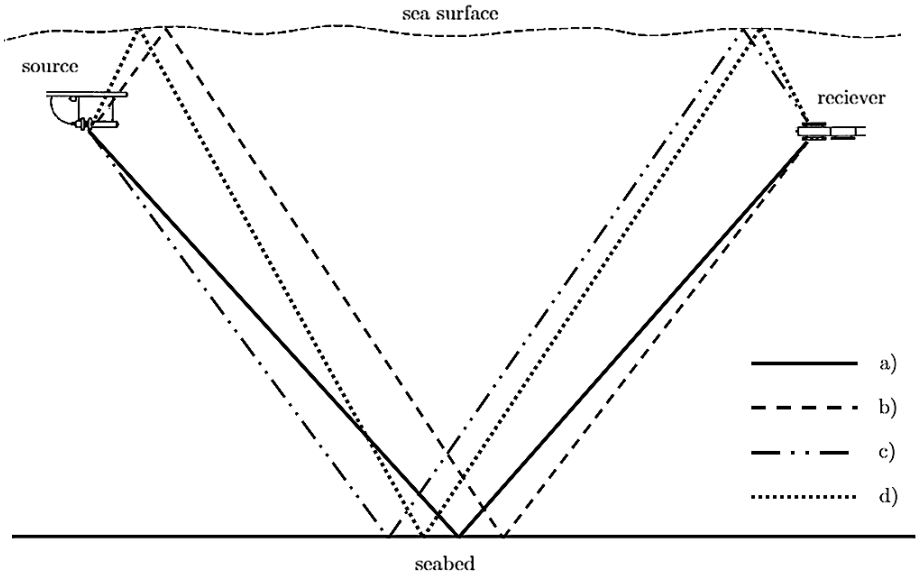

Figure 2.5 – *Source and reciever ghosts in marine streamer acquisition. Event a) is the primary ray path from source to receiver. Event b) includes source ghost reflection from sea surface, while event c) includes reciever ghost from the sea surface. Event d) contains both source and reciever ghost reflection*

To model the ghost and its effect on the primary wave field we can imagine the source ghost reflections to originate from a source mirrored against the sea surface, and the receiver ghosts as if recorded at a reciever mirrored against the sea surface, as illustrated in **Fig. 2.6**, to derive the additional travel times for the two.

Simple trigonometry gives additional travel distance $X_s = 2Z_g cos\phi$ for source ghost reflection and $X_r = 2Z_g/cos\phi$ for reciever ghost reflection, yielding additional travel times τ_s and τ_r for source and receiver ghost respectively

$$\tau_s = \frac{2Z_g cos\phi}{c} \tag{2.6}$$

and

$$\tau_r = \frac{2Z_g}{cos\phi \cdot c} \tag{2.7}$$

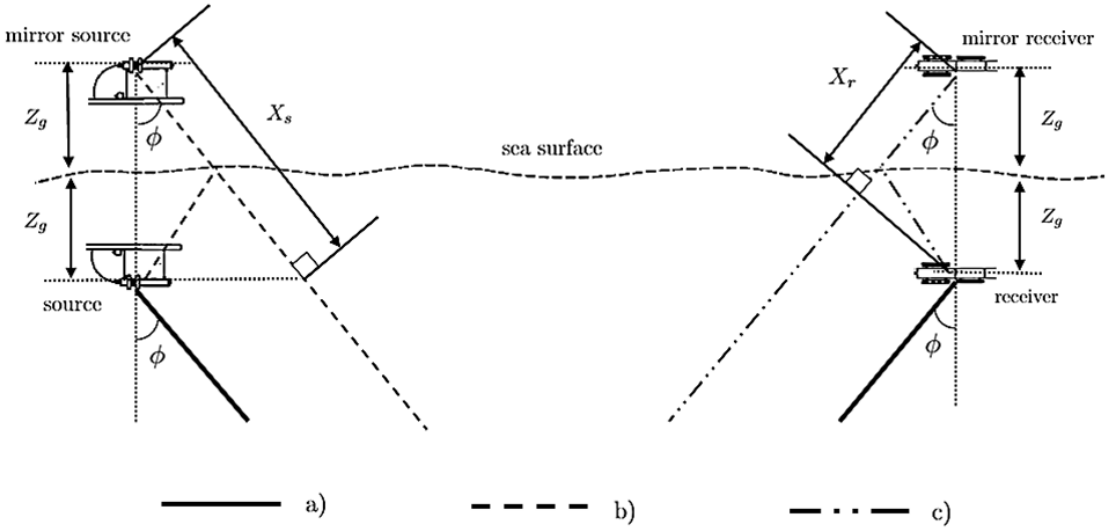

Figure 2.6 – *Source and receiver ghost additional travel distance illustrated using mirror source and mirror receiver concept. Z_g is source and receiver depth, and ϕ is incidence angle. Event a) indicates primary raypath, b) includes source ghost reflection, and event c) includes receiver ghost. X_s and X_r indicates additional travel distance for source and receiver ghost reflection respectively.*

If we further assume bulk density and pressure wave velocity values for air and water, $\rho_{air} = 1.225\,kg/m^3$, $\rho_{water} = 1000\,kg/m^3$, $V_{p,air} = 330\,m/s$ and $V_{p,water} = 1450\,m/s$ and insert in Eq. 2.3 we can calculate the expected general reflection coefficient at the free surface:

$$R = \frac{v_{p,air} \cdot \rho_{air} - v_{p,water} \cdot \rho_{water}}{v_{p,air} \cdot \rho_1 + v_{p,water} \cdot \rho_{water}} = \frac{1.225 \cdot 330 - 1000 \cdot 1450}{1.225 \cdot 330 + 1000 \cdot 1450} = -0.99949 \approx -1 \quad (2.8)$$

The reflectivity will vary slightly with regards to salinity, temperature and ocean swell, but is often assumed to be -1, allowing the free surface to act as a perfect acoustic mirror. Using this assumption and the derived additional travel times we can express the far field composite response vertically for zero incidence at a distance R below source deployed at a depth Z_g as expressed by Landrø (2011):

$$s(t) = \frac{1}{R}p(t - \frac{R}{c}) - \frac{1}{R_g}p(t - \frac{R_g}{c}), \quad (2.9)$$

where $p(t)$ denotes the notional air gun signal, c is water water velocity while R_g represents the travelling distance for the ghost, $R_g = R + 2Z_g$. Fourier transform of the source term and ghost term, yields

$$\mathscr{F}\{\frac{1}{R}p(t-\frac{R}{c})\} = \frac{1}{R}P(\omega)e^{\frac{-i\omega R}{c}} \tag{2.10}$$

and

$$\mathscr{F}\{\frac{1}{R_g}p(t-\frac{R_g}{c})\} = \frac{1}{R}P(\omega)e^{\frac{-i\omega(R+2z_g)}{c}} \tag{2.11}$$

respectively, when $R_g \approx R$ in the ghost term denominator, valid for $R >> z_g$. The source term $\frac{1}{R}P(\omega)$ is common in Eq. 2.10 and 2.11, allowing Eq. 2.9 can be written as:

$$S(\omega) = \frac{P(\omega)}{R}e^{\frac{-i\omega R}{c}}[1-e^{\frac{-i\omega(2z_g)}{c}}] \tag{2.12}$$

By isolating the last term of Eq. 2.12 we can express the ghost function

$$G(\omega) = 1-e^{\frac{-i\omega(2z_g)}{c}} \tag{2.13}$$

that rewrites to the power spectrum as a function of frequency:

$$\mid G(f) \mid = \mid 2sin\frac{2\pi f z_g}{c} \mid \tag{2.14}$$

As $\mid sin(x) \mid \in [0,1]$ it follows that $\mid G(f) \mid \in [0,2]$ in Eq. 2.14, meaning the zero incidence ghost effectively doubles the signal amplitude at maximum value and zero amplitude at minimum value. Sine function with argument set to zero gives the notch frequencies f_{min}, while argument set to $\pi/2$ gives strengthening of the amplitude in frequencies f_{max}:

$$f_{min} = \frac{c}{2z_g}n, \;\; n = 0,1,2,3,... \tag{2.15}$$

$$f_{max} = \frac{c}{2z_g}(n-\frac{1}{2}), \;\; n = 0,1,2,3,... \tag{2.16}$$

It follows from Eq. 2.15 that the first notch always can be expected at 0 Hz, regardless of z_g, and hence will both low and high frequencies be directly limited by the ghost in conventional marine acquisition.

If source and receiver are not towed at same depth, more notches are introduced to the frequency spectrum as the source and receiver notches will not coincide. Similarly, by configuring source and receiver at same depths, constructive summation yields a four times amplitude strengthening at the f_{max}.

In addition to signal cancelling at f_{min}, the rounded shape of the squared sinus term in Eq. 2.14 results in attenuated frequencies on both sides of the actual notch, as illustrated in **Fig. 2.7** for ghost function at three different depths. This relation between the acquisition configurations and the frequency content of the acquired data illustrates the importance of carefully considering survey objective when designing the acquisition. For high-resolution imaging of shallow subsurface, such as in marine geohazard studies, particular emphasis is set to extend the high-frequencies in order to resolve thin gas traps or over-pressured sand layers. For a depth of 6 m Eq. 2.15 and $c = 1500\,m/s$ gives second ghost notch at 125 Hz yielding high frequency content and high resolution. However, a wide range of the important low-frequency amplitudes are severely reduced, limiting penetration and impeding ideal wavelet shaping. A shallow towed streamer will also be more influenced by ocean swell than a streamer towed at deep, decreasing signal-to-noise ratio, potentially jeopardizing the quality of the acquired data (Özdemir et al., 2008). A towing depth of 24 m yields strong amplitudes in the low frequency range, allowing for deep structural imaging and improved seismic inversion (Kroode et al., 2013). However, the second ghost notch at 31.25 Hz strongly restricts the seismic resolution according to Reyleigh's criterion, effectively illustrating that a survey with both low-frequency and high-frequency objectives is difficult to achieve with conventional streamer technology due to the seismic ghost (Amundsen and Landrø, 2010b).

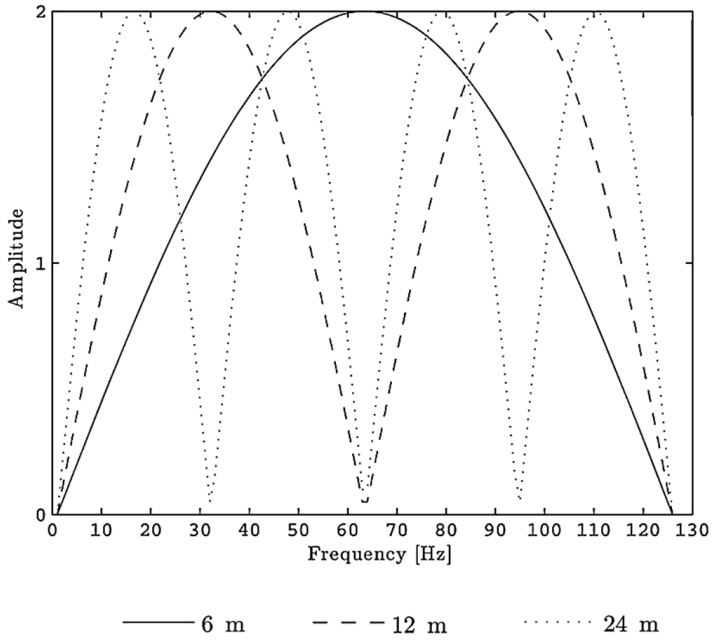

Figure 2.7 – *Ghost notch modelling. 6m, 12m and 24 m depth using Eq. 2.14 with* $c = 1500m/s$

2.5 Broadband acquisition technology

Conventional streamer data is limited by the ghost effect both in ends of the seismic frequency spectrum. Broadband technology is aiming to provide ghost free data solutions in order to improve resolution and penetration by eliminating, or strongly reducing, the impact of the ghost.

Many different physical and mathematical concepts have been applied in the pursue for ghost free acquisition in the last half century. Wavefield separation was introduced by Sønneland (1986) and describes the theoretical decomposition of the recorded wavefield into up- and downgoing components, forming the foundation of most broadband technology. This concept was realized in the Over/under towed-streamer technology launched by WesternGeco in the mid 2000's. Over/under acquisition aims to provide broadband data by combining advantages of shallow and deep cable arrangement using streamers towed in pairs at two different depths. (Özdemir et al., 2008) Altough conceptually straight forward, similar acquisition designs had earlier suffered from poor alignment control between the vertically paired cables, yielding less-than desirable results. Successfull implementation was ultimatly enabled by developments in streamer technology allowing precise steering and positioning, illustrating the significance of innovation and technology maturation in the quest for broadband data.

2.5.1 Dual streamer technology

The true commercial breakthrough of broadband acquisition technology is often credited to Petroleum Geo-Services and the introduction of their GeoStreamer. Presented in 2007, the dual component technology allow measurements of both the pressure and the velocity field, to utilize the complementary information given in the two recordings. The directional velocity sensors permit measurements of the down-going velocity wavefield with equal polarity as the up-going, enabling separation of the two wavefields, and effective recognition of the receiver ghost (Carlson et al., 2007). For hydrophone measurements the ghost function and its frequency spectrum as derived in Ch. 2.4 now denoted G_- we have

$$G_- = 1 - e^{-i\omega\tau} \tag{2.17}$$

and

$$|G_-(f)| = 2|\sin(\frac{2\pi f z}{c})| \tag{2.18}$$

with, receiver depth z, water velocity c, angular frequency ω and ghost delay time $\tau = 2z/c$ as derived from **Fig. 2.6**. Since the particle velocity measurements record the

difference between upgoing and downgoing vertical wavefield, the corresponding particle velocity ghost function G_+ becomes

$$G_+ = 1 + e^{-i\omega\tau} \tag{2.19}$$

with a resulting frequency spectrum

$$|G_+(f)| = 2|\cos(\frac{2\pi f z}{c})| \tag{2.20}$$

As illustrated in **Fig. 2.8** notch frequencies for pressure recordings and particle velocity are perfectly out of phase. Hence, the two measuremets yield complimentary information and may be combined to a notch free signal.

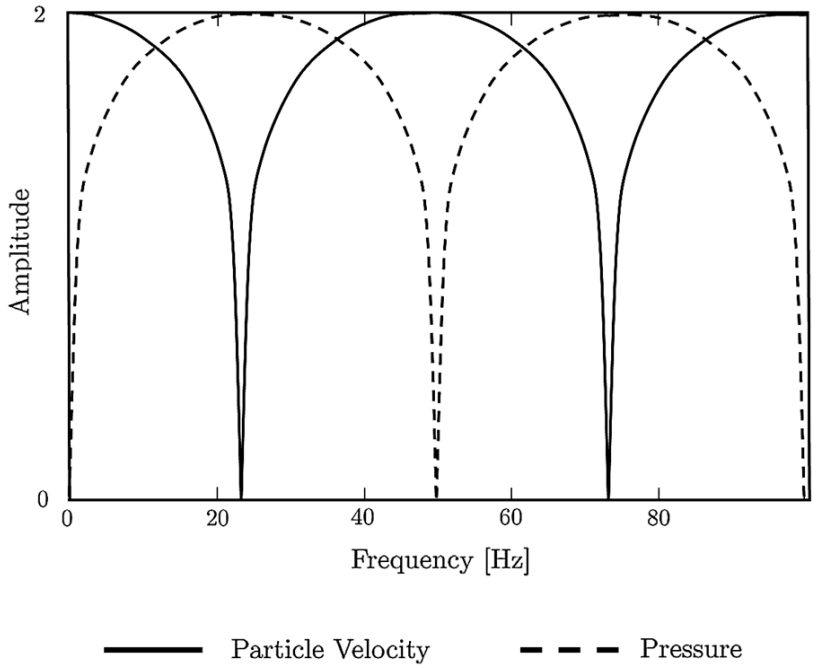

Figure 2.8 – *Pressure and particle velocity ghost notches for 15 m depth and water velocity 1500 m/s*

If we denote the zero offset hydrophone pressure measurements and geophone particle velocity measurements P and Z respectively and reflection response of R we can express hydrophone measurements

$$P \sim RG_- \tag{2.21}$$

and the geophone measurements as

$$Z \sim RG_{+}. \tag{2.22}$$

For scaling, Eq 2.21 and Eq. 2.22 can be combined using

$$\frac{1}{2}(P + Z) = R. \tag{2.23}$$

Tenghamn et al. (2007) discuss the practical limitations of the early dual-streamer technology, as initial implementation of motion sensors in marine towed streamer acquisition proved challenging. Poor signal-to-noise ratio restricted useful applications as the lowest frequencies were severely affected by strumming noise in the cables. However, by using the relation between P and Z

$$Z \sim \frac{G_{+}}{G_{-}}P. \tag{2.24}$$

the P-data allows direct estimation of the Z-data for the particle velocity measurements with low signal-to-noise ratio. This P-Z summation method is performed in practice by filtering the noise dominated low frequency Z-data, before using Eq. 2.24 to compensate for the filtered data. The high frequency Z-data with acceptable signal-to-noise ratio can merged with the estimated data, before merging with the P-recordings to yield true broadband frequency content exceeding the conventional bandwidth range.

2.5.2 Variable-depth streamer technology

Conventional marine streamer acquisition tow cables at a constant depth, consequently resulting in a distinct receiver ghost at the corresponding frequency. Variable-depth streamer technology aims to achieve the best possible signal-to-noise ratio by towing the streamer deep, but using a depth profile that varies with offset as illustrated in **Fig. 2.9**. The concept seeks to create notch diversity in the frequency spectrum as the notch frequency varies with receiver depth along the streamer profile.

The benefits of notch diversity from non-flat streamer profile was investigated already in the 80's by Ray and Moore (1982) who patented a slant streamer marine acquisition system. The variable-depth streamer concept is today applied successfully in CGG's commercial broadband solution BroadSeis, using a curved profile down to target towing depth where the streamer flattens out. The profile is optimized with a larger slope at near offsets to yield sufficient diversity for shallow reflectors, and favours high frequencies in the curved section while low frequencies are favoured in the flat, deep section (Soubaras and Lafet, 2011).

The variable depth streamer does however introduce a set of new challenges in the assessment of the acquired data, as the variable depth of recordings need to be accounted

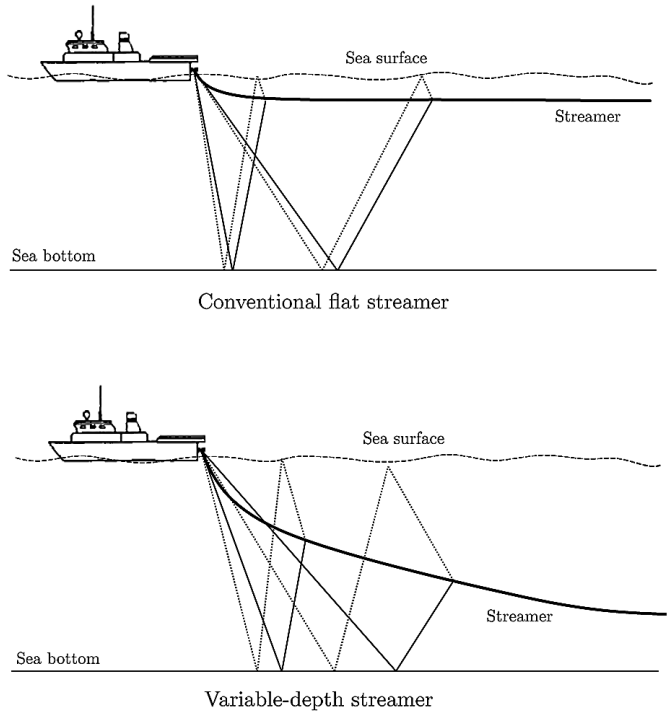

Figure 2.9 – *Conventional flat streamer acquisition compared to variable-depth streamer acquisition. Solid lines indicate primary reflection, dotted line indicates ghost reflection.*

for in the analysis to yield correct amplitudes for given offsets. This matter is critical in advanced reservoir characterization depending on reliable positioning and angle dependencies such as AVO studies and repeated seismic acquisition for reservoir monitoring. A development of great importance for the use of BroadSeis variable depth streamer has therefore been the ability to re-datum data to a level of preference. As described by Poole (2013), this allow recordings to be positioned at given levels such as the sea surface or for depths coinciding with previous acquisition streamer position in the case of repeated seismic monitoring surveys.

2.5.3 Multicomponent streamer technology

In addition to ghosts restraining frequency content in the data, a setback of commercial marine acquisition is the typical streamer separation being wider than advantageous in order to favour more efficient operation. Multicomponent streamer technology introduces measurements of both pressure and 3D particle acceleration and serves as the foundation of WesternGeco's Isometrix broadband system, aiming to account for both of these constrains. WesternGeo's Nessie-6 streamer provides pressure and micro-electromechanical system-based measurements of acceleration as illustrated in **Fig. 2.10**. The acceleration data can be used to derive the pressure gradient field, and solve for the missing frequen-

cies caused by the ghost notch, while the three-directional measurements can reconstruct the upgoing wavefield between streamers, increasing spacial resolution (Bunting et al., 2013).

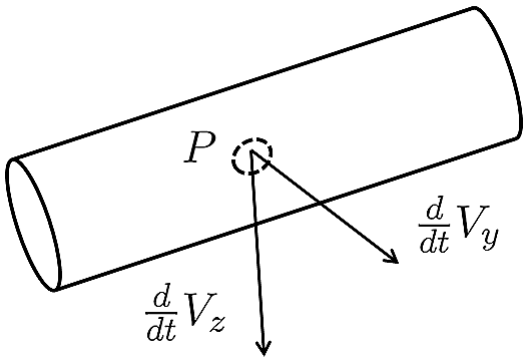

Figure 2.10 – *Nessie-6 streamer measurements providing pressure data p and both inline and crossline acceleration.*

Using the Nessie-6 measurments IsoMetrix derive vertical velocity V_z and crossline velocity V_y, allowing for PZ-summation as discussed in Ch. 2.5.1. The IsoMetrix system does not specifically target low frequency estimation as the GeoStreamer does, but aims to overall suppress the receiver ghost using the complimentary information given by the pressure and particle velocity. This allows deeper towing, and hence more low frequencies and a consequent broader frequency band. In addition, the integrated IsoMetrix system seeks to account for sparse crossline data density, resulting from the large streamer separation distance, using the the gradient of the pressure wavefield. WesternGeco implemented the Generalized Matching Pursuit algorithm as described by Özbek et al. (2010), reconstructing and deghosting the seismic wavefields simultaneously, arguably giving superior interpolation results in crossline direction with the three component data compared to pressure component data only.

The broadband technology provided by the major seismic contractors emphasizes the attention and effort persistently dedicated to development of ghost free data solutions. Implying a future trend in seismic acquisition, the oil & gas industry may expect to see a shift towards new acquisitions delivering ghost free data as a standard in the time to come. However, improved data quality may not always defend a costly broadband acquisition for a client. For many of the well-explored basins in mature areas, decent quality seismic data is already available. Parallel to the acquisition technology development, research has accordingly been put into solutions that may provide broadband data without reacquiring new seismic, through targeted processing on the ghosted data to improve the resolution.

2.6 Processing of seismic data

The purpose of seismic processing is to improve data imaging using targeted computer operations that increase the signal-to-noise ratio and shift the reflection readings to their true position according to the subsurface. A processing workflow is developed uniquely for each survey depending on the acquisition parameters, survey target and resources available. A simplified conventional workflow is illustrated in **Fig. 2.11** emphasizing the main objectives of seismic processing.

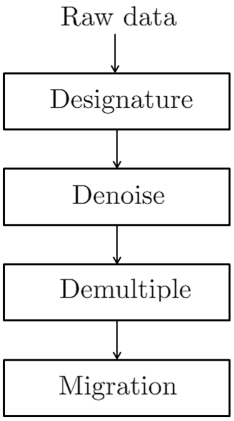

Figure 2.11 – *Conventional seismic processing workflow*

In modern commercial processing each objective typically compromises a complex series of mathematical algorithms, parameter tests, domain transformations and sorting techniques in order to optimize the operation for each unique dataset. When assessing seismic records the interpreter should always be familiar with the processing applied to the data. Different algorithms may alter the appearance, and content, of the data in a way that could lead to pitfalls in the reservoir characterization. Seismic processing of commercial data is usually performed by dedicated processing contractors with expertise, software tools, and computational capacity to work with the large data volumes acquired in a seismic survey. The different processing techniques are often developed and optimized in-house, and are aggressively protected by patents to give the contractor competitive advantages in the market.

A fundamental assumption in many processing algorithms is that the recorded seismic signal can be expressed as a convolution between the emitted wavelet and the impulse response of the earth

$$y(t) = w(t) * f(t) \tag{2.25}$$

where $y(t)$ is the recorded signal, $w(t)$ is the emitted wavelet and $f(t)$ is the impulse response we seek to know. We may therefore theoretically design inverse filters for the

wavelet and noise in our data. Time-varying Wiener shaping filters allows conversion from the input to any desired output as derived by Robinson and Treitel (2000):

$$\begin{bmatrix} r_0 & r_1 & ... & r_{n-1} \\ r_1 & r_0 & ... & r_{n-2} \\ r_2 & r_1 & ... & r_{n-3} \\ ... & ... & ... & ... \\ r_{n-1} & r_{n-2} & ... & r_0 \end{bmatrix} \begin{bmatrix} a_0 \\ a_1 \\ a_2 \\ ... \\ a_{n-1} \end{bmatrix} = \begin{bmatrix} g_0 \\ g_1 \\ g_2 \\ ... \\ g_{n-1} \end{bmatrix} \tag{2.26}$$

Here r is the autocorrelation of the input wavelet, g is the crosscorrelation of the desired output and the input wavelet, and a the filter coefficients. The Wiener matrix equation allows filter design for a wide range of applications, however the theory rests on a set of assumptions with important implications that needs to be discussed. The convolutional model assumes normal incidence wave propagation for plane layers of constant velocity, with a known stationary waveform that is excluded from frequency dispersive effects or losses of amplitude due to spreading or absorption. Noise is also considered negligible. In actuality these assumption may not be valid, but the widespread successful application of the convolution and deconvolution in geophysical signal theory states their obvious value for processing algorithms.

2.6.1 Designature

The preferred seismic wavelet for an interpreter assessing data is symmetrically zero-phased. The far-field signature recorded, however, compromises minimum phase wavelet from the air gun and includes residual bubble energy and energy reflected at the sea surface. Designature aims to ideally convert data from raw seismic wavelet into a sharp symmetrical zero-phased wavelet, as illustrated in **Fig. 2.12**.

Designature is performed by deconvolving the bubble signature with the raw seismic wavelet, zero-shift the wavelet using filtering, and often invert the polarity. To predict the deconvolution the far-field signature is assumed known, being either measured from acquisition or modelled. Different measurement techniques exist, including notional-source method and ministreamer inversion method as described by Landrø (2011). Far-field signature modelling inputs acquisition configuration such as array depth, and gun volumes and in addition to sea column properties such as temperature and water depth. Today, most acquisition contractors will provide the far-field as a part of the delievery to clients and processing contracts.

2.6.2 Denoise

Seismic data from marine acquisition is usually affected by swell noise, hydrostatic pressure variation noise, tugging, cavitation noise and seismic interference. Attenuation of

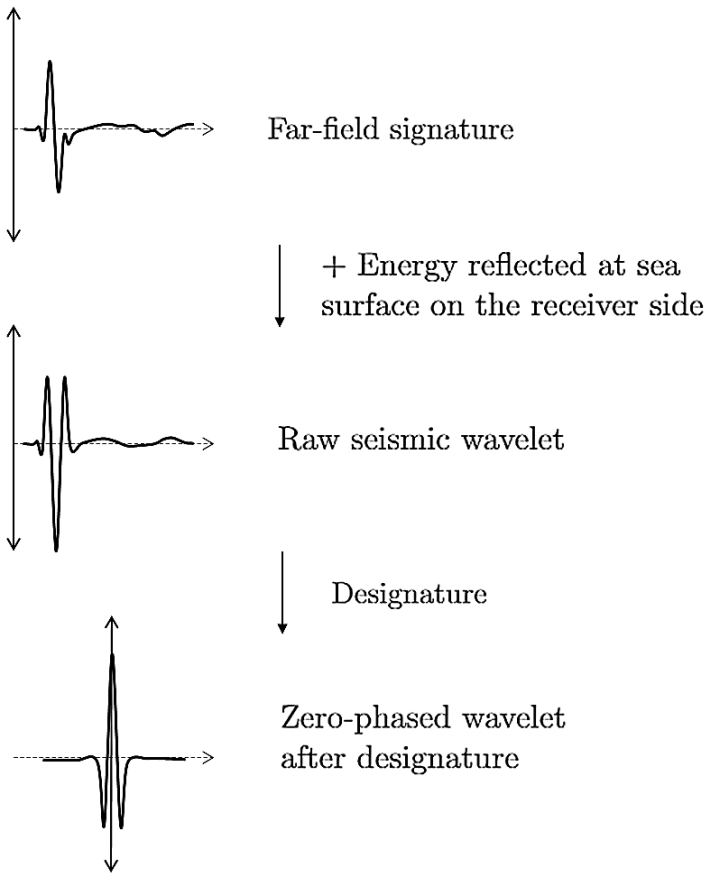

Figure 2.12 – *Conventional designature. Top: Far-field signature compromising source signature, energy reflected at sea surface on the source side and residual bubble. Mid: By adding energy reflected at sea surface on reciever side to the far-field signature we yield the raw seismic wavelet. Bottom: Successful designature provides a zero-phased wavelet.*

noise in the seismic data is an important, yet complicated objective in processing. The de-noising algorithms typically involve a mathematical transformation into another domain where the desired and the undesired events are distinguishable, such as Radon, $f-k$ or Fourier, allowing convenient filter design (Elboth and Hermansen, 2009). **Fig. 2.13** illustrates a simple attenuation algorithm of hydrostatic pressure variation attenuation in $f-x$ domain. A physical understanding of the individual sources and origins of noise artifacts improve our to ability to choose appropirate algorithm and distinguish reflection readings from noise in our seismic data by recognizing patterns and typical features of the noise.

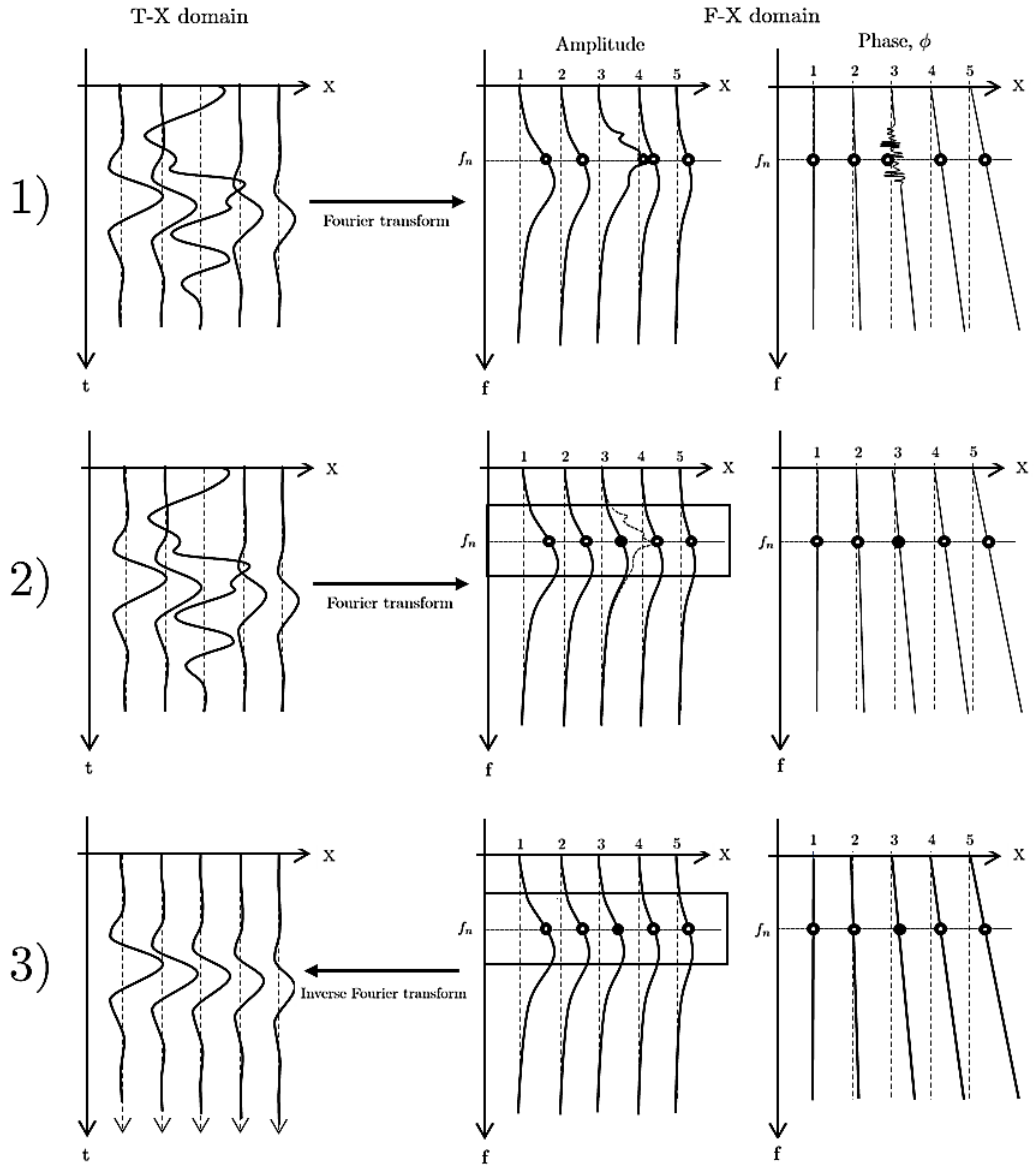

Figure 2.13 – *Simple noise attenuation algorithm in $f-x$-domain. 1) A seismic gather with a trace affected by swell noise is Fourier transformed into $f-x$-domain and displayed in amplitude and phase to ensure preservation of the anomaly in the new domain. 2) A computational window is defined over the transformed data and set to identify data points exeeding a defined threshold median. Identified data points are flagged and replaced with interpolated values from the other traces. 3) The data is ultimately inversely transformed back to $t-x$ domain yielding noise attenuated traces.*

2.6.3 Demultiple

In seismic data a multiple is energy which has at least one downward reflection in its travel path, and occur because an interface is a bidirectional reflector; the down-going energy is reflected towards the surface, but the up-going wavefield is also reflected back into the subsurface, as illustrated in **Fig. 2.14**. Multiples can consequently be differentiated on whether the downward reflection is due to to the acoustic impedance contrast between geological layers or the free water surface.

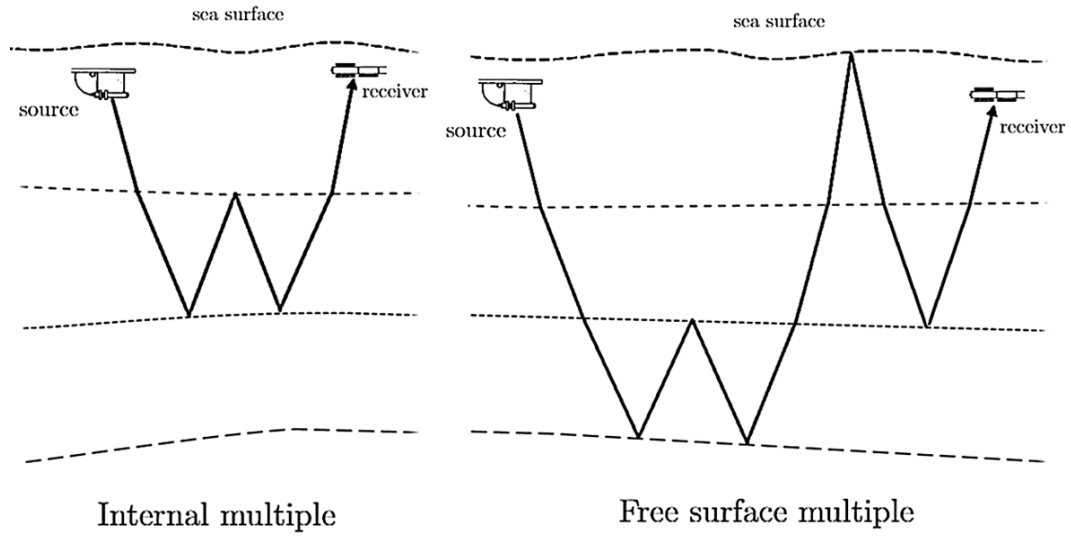

Figure 2.14 – *Multiples in marine seismic acquisition. Left: Internal mutiple. Right: Free surface multiple.*

Sheriff (2002) distinguish between long-path and short-path multiples. Long-path multiples arrives as a distinct event in the reflection records whereas a short path multiple interferes with the primary signal. Hence, multiples can appear indistinguishable from the primary reflections on the seismic record posing a threat to structural interpretation, but can also jeopardize quantitative analysis such as AVO-modelling due to deformation of the wavelet.

Multiples may be attenuated using many different techniques, including FK-filtering after normal moveout correction, or deconvolution methods, depending on the subsurface geology, noise in dataset and computational power. A popular free surface demultiple technique in commercial processing is predictive deconvolution as derived by Robinson and Treitel (2000), Ch. 12, followed by a spiking deconvolution.

By allowing crosscorrelation vector g in 2.26 to take the form of a time-advanced configuration of the input series, setting g as the autocorrelation function of the input data delayed with the lag α we get the predictive deconvoltion matrix equation

$$\begin{bmatrix} r_0 & r_1 & ... & r_{n-1} \\ r_1 & r_0 & ... & r_{n-2} \\ r_2 & r_1 & ... & r_{n-3} \\ ... & ... & ... & ... \\ r_{n-1} & r_{n-2} & ... & r_0 \end{bmatrix} \begin{bmatrix} a_0 \\ a_1 \\ a_2 \\ ... \\ a_{n-1} \end{bmatrix} = \begin{bmatrix} r_\alpha \\ r_{\alpha+1} \\ r_{\alpha+2} \\ ... \\ r_{\alpha+n-1} \end{bmatrix} \tag{2.27}$$

Long-path multiples appear on the autocorrelation function as distinct waveforms which are separated by quiet zones. Short-path multiples appear on the autocorrelation function in the form of decaying waveforms which are not separated by any noticable quiet intervals. If we then allow the crosscorrelation vector g in 2.26 to be a zero-lag spike we get the spiking deconvolution matrix equation.

$$\begin{bmatrix} r_0 & r_1 & ... & r_{n-1} \\ r_1 & r_0 & ... & r_{n-2} \\ r_2 & r_1 & ... & r_{n-3} \\ ... & ... & ... & ... \\ r_{n-1} & r_{n-2} & ... & r_0 \end{bmatrix} \begin{bmatrix} a_0 \\ a_1 \\ a_2 \\ ... \\ a_{n-1} \end{bmatrix} = \begin{bmatrix} 1 \\ 0 \\ 0 \\ ... \\ 0 \end{bmatrix} \tag{2.28}$$

The autocorrelation is the main input to the deconvolution design, meaning the success of attenuation of multiples using deconvolution is primarily dependent on the ability of autocorrelation to identify the multiple periodicity.

2.6.4 Migration

The objective of migration is to move reflections to their true subsurface positions and collapse diffractors, effectively increasing spatial resolution (Yilmaz, 2001). Migration aims to reverse wave propagation effects in order to obtain clear images of the subsurface, and will ideally yield seismic data with correct amplitude, phase and position. The inital foundation of migration algorithms is the wavefield extrapolation modelling. Concidering a wavefield $P(x, z, t)$ in a media with constant acoustic impedance the 2D scalar wave equation yields:

$$(\frac{\partial^2}{\partial x^2} + \frac{\partial^2}{\partial z^2} - \frac{1}{v^2}\frac{\partial^2}{\partial t^2})P(x, z, t) = 0 \tag{2.29}$$

In practice Eq. 2.29 is solved either using integral solutions, finite-difference solutions or using frequency-wavenumber implementation. After wave propagation modelling an imaging algorithm is usually applied to the data, using cross-correlation of two extrapolated wavefields. All migration algorithms require a high quality velocity model, and a careful model building is critical. The more accurate velocity model, the better the migration results.

Algorithms migrating seismic data are highly complex and requires great computational power, yet advances in technology, and computer science in particular, has allowed development of several reliable migration algorithms for commercial purposes. These include the classic Kirchhoff time migration, finite difference migration, frequency-wave number migration and the emerging reverse time migration. The choice of algorithm is usually a trade off between data complexity and computational power available.

Kirchhoff migration is considered a reliable algorithm, effectively illustrating the objective of the seismic migration. Considering a hyperbolic diffraction curve in a zero-offset section, Kirchhoff migration sum the amplitudes along the hyperbola and collapse the curve into a single point at apex. The zero-offset section can be considered as a set of diffractors superpositioned at each time sample according to Huygens' principle. The diffractors interfere, forming coherent events, while individual diffractions are preserved at discontinuities such as faults or terminating layers. At each separate output time migrated position the amplitudes of the input zero-offset time data can be summed along a series of hyperbolas according to input velocity model. Maximum amplitudes will occur at the true migrated event, while the amplitudes elsewhere will be minimal.

2.7 Broadband processing of conventional data

Broadband seismic data may be obtained by reducing ghost effects in acquisition stage as described in Ch. 2.5. A processing based broadband solution however, is arguably more cost effective, not requiring extra acquisition effort, and is applicable to the complete existing legacy data library acquired by conventional streamer technology.

Attempts to suppress the seismic ghost in seismic reflection records was discussed in seismology already in the early 1960s. Lindsey (1960) applied a linear filtering operator to eliminate the seismic ghost reflection on magnetic tape recordings using a single-loop feedback system. Hammond (1962) derived a method to reduce the ghost energy by composing two magnetic tapes obtained from predetermined shot depths in the same shot hole. A more modern approach to deghosting marine data was later suggested by Sønneland et al. (1986) who introduced the concept of decomposing the recorded wavefield into up- and downgoing components using a vertical array in the receiver geometry.

A traditional approach to receiver deghosting has been to include the zero-offset receiver ghost as derived in Eq. 2.13 into the far-field signature and perform 1D deconvolution of the dataset at preprocessing stage. A simple 2D operator for removing the receiver ghost is the $x-y-t$ domain pseudo-differential operator D

$$D = \frac{1}{1 + re^{2iz\sqrt{\frac{w^2}{c^2 - {k_x}^2 - {k_y}^2}}}} \tag{2.30}$$

where r is free surface reflection coefficient, c is water p-wave velocity, z is reciever depth, ω is angular frequency and k_x and k_y is the horizontal and vertical wavenumber respectively (Zhou et al., 2012). Typically applied to shot records in the $f-k$ or $f-p$ domain the psuedo-differential operator offers simple and quick implementation. However, due to the variable nature of receiver depth r in under normal marine conditions, the mathemathical unstable behaviour due to near singularity, and edge effects given by the inverse transformations, strongly limit the application of the operator. More sophisticated deconvolution methods have been proposed by Amundsen et al. (2013) among others, who dervied a spatial deghosting operator in the frequency domain using deterministic deconvolution.

Soubaras (2010) offers a different approach to broadband processing by suggesting a dual-input post-stack joint deconvolution method, arguing that general signal processing theory propose applying deconvolution of redundant measurements with variable wavelet after the data stack. The principle of the method is to perform a migration together with a mirror migration, before joint deconvolving the two images. The technique was orginally developed for variable-depth streamer data, but can also be extended to conventional streamer data. The technique however implies preservation of the ghosted wavelet throughout the complete processing workflow until the imaging stage. This major challenge drastically introduces strict restraints in the algorithms, potentially deprioritizing other important targets in the processing workflow.

A $x-t$ domain approach is presented by Beasley et al. (2013) using the wave equation to simulate up- and down-going wavefield propagation between receivers and the free surface to derive wavefield separation. The authors suggest that the upgoing, deghosted wavefield can be computed iteratively by first evaluating a Kirchhoff integral over earlier values of the upgoing wavefield, which is then subtracted from the recorded pressure wavefield, yielding the next value of upgoing wavefield. In a recent paper Robertsson and Amundsen (2014) derive a similar method, also assuming causality to predict the downgoing wavefield from the upgoing wavefield using a wave-equation propagator. The authors chose a time-space domain finite-difference solution to the wave equation with pressure field boundary conditions. The method delievers promising results on both simple and complex synthetic data but show sensitivity to variations in streamer depth, introducing ringing noise in the deghosted solution.

CGG is currently utilizing two different deghosting techniques to their client data. Wang and Peng (2012)'s bootstrap technique and Poole (2013)'s least squares linear Radon method are both showing encouraging results for successful application of broadband processing on conventional streamer data.

Chapter 3

Offshore shallow geohazards

In the hydrocarbon production, a geohazard is any geological phenomenon or process that may pose a threat to the operation, the installation, the environment or to human safety (Campbell, 2003). In ISO17776:2000 the International Organization for Standardization defines:

> **geohazard:** A geological state that represents or has the potential to develop further into a situation leading to damage or uncontrolled risk.

Offshore shallow geohazards may be specifically evaluated by considering the seabed and the rock volume down to 1 ms two-way time below the seabed. Consequently offshore shallow geohazards can include both sea floor geological hazards such as fault scarps, slumping, mass sediment movement and reefs, and subsurface geological hazards such as faults, gas-charged sediments, gas hydrates and shallow water flow (Dutta et al., 2010). Both local and regional geologic site conditions having the potential of developing into a failure event causing damage to health, environment or assets, constitute a geohazard threat regardless if triggered by geological processes or the operation itself.

Offshore geohazards were recognized by the oil & gas industry already in the 1970s following impact of hurricane Camille in 1969. In the open Golf of Mexico, the storm created offshore mudslides rapidly lowering the ocean floor, causing damages estimated to 100 million USD to three production platforms and their associated network alone. The resulting acknowledgement of potential sea floor instabilities in site selection introduced the concept of proactive geohazard risk management. Throughout the 1980s and -90s, oil & gas exploration and field development expanded rapidly into immature offshore areas with deeper water, more complex geological and tectonical settings presenting new geohazard challenges (International Association of Oil & Gas Producers, 2009). Increased attention divided to human and environmental safety has since then made offshore geohazards an important topic of research in order to develop best practices and industry standards to secure a safe and efficient performance while reducing the operational costs to related to accidents. A large number of major oil companies

explicitly define reduction of geohazard-related risks among their current top research priorities (Solheim et al., 2005).

Geohazard assessment is a complex, multidisciplinary challenge involving geology, sedimentology, geophysics, and geotechnics, and seek to identify, map and quantify the risks in volume of interest. The assessment considers not only the conventional subsurface targets of interest such as water depth, seafloor topography, lithology, stratigraphy and pressure gradients, but also typically evaluate the frequencies and magnitudes of the active geological processes in the area (Campbell, 2003). The marine engineering geophysicist's role is hence to apply the appropriate geophysical tools and utilize data to assess these parameters in a quantitative manner.

3.1 Mass-transport complexes

Mass-transport complexes, or underwater landslides, slumps or debris deposits, are massive expressions of slope failure and play a fundamental role in modifying and shaping submarine morphology in slope and deep-water basins of the world. The mass-transport complexes form a key stratigraphic component of many margins and may in some settings constitute up to 70 % of the entire slope and deep-water stratigraphic column (Weimer and Shipp, 2004). The slope failure depend on sedimentation rate, pressure regimes, temperatures, slope morphology and sediment strength among others. The failure may be triggered by both geological activity and human operation, posing great threat to platform anchoring, subsea and drilling installations, and pipelines in the offshore hydrocarbon production (Chopra and Marfurt, 2007, Ch. 14).

In areas with varying deposition or erosion, active faulting or submarine channel topography, the increased gradient account for greater risk of mass-transport deposits. The slope failure may be gradually forced by erosion due to over-steepening, or may be trigged by earthquakes, volcanic activity, storms and tsunamis. Even human induced changes in pore pressure by production and change in loading conditions from subsea installations, rockfill support and platform anchoring may activate the failure. Large mass-transport complex deposits are observed along the continental slopes offshore, and by mapping them on and near the seabed we may evaluate the frequency, the size, and the position of the remaining slide scarps in order to quantitatively risk different slope failure scenarios in the geohazard assessment (International Association of Oil & Gas Producers, 2009).

3.2 Shallow-water flow

Shallow-water flow was first reported in 1985 during drilling in the Gulf of Mexico and has since then been frequently encountered in many deepwater petroleum provinces including North Sea, Norwegian Sea, West Africa, Caribbean and Caspian Sea. Although usually

found at water depths greater than 500 m, at well depths more than 400 m below the seabed, shallow-water flow has been encountered both in shallower water and closer to seabed during offshore drilling (Judd and Hovland, 2009, Ch. 11.3.3).

Shallow-water flow is considered the single most significant drilling hazard in deepwater settings (Dutta et al., 2010). They are prevalent in basins with high depositional rates and result from rapid burial of sand and silt followed by differential compaction and de-watering, as illustrated in **Fig. 3.1**. A shallow-water flow is formed when sand-rich deposits from turbidity flows or sea level change become sealed with a condensed zone from shale or gas hydrates. The water-sand suspension is trapped by the condensed zone, and with following deposition and burial, the weight of the overlying sediment results in the build-up of geopressure by disequilibrium compaction. With sufficient burial the pressurized water sand slurry will eventually result in natural expulsion and flow (Mallicks and Dutta, 2002). The nature and magnitude of the shallow water flow hazards depend on the seal strength, lithology, thickness, distribution of seals and bouyancy effects.

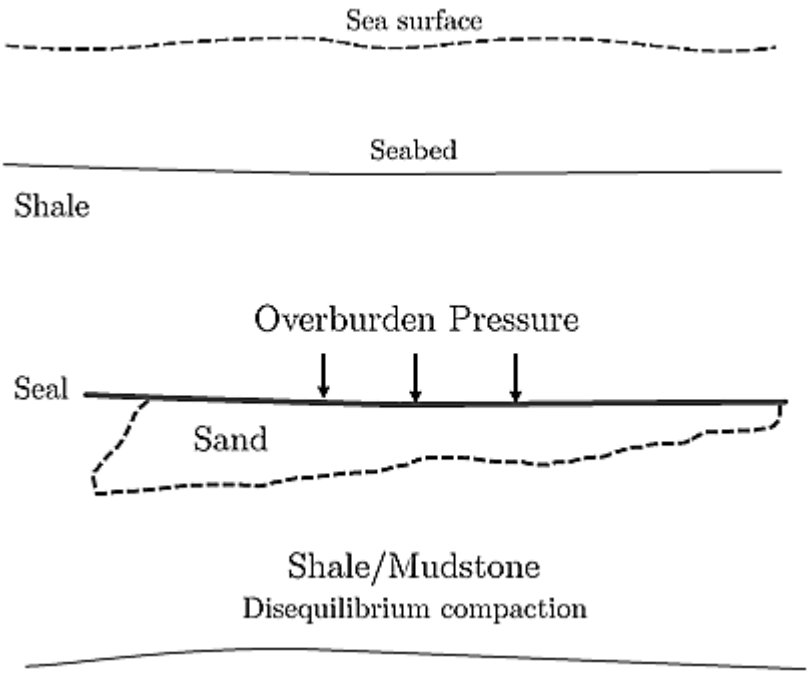

Figure 3.1 – *Formation mechanism of Shallow-water flow sand layer (Figure modified after Mallicks and Dutta (2002))*

Shallow-water flow hazards require effective mitigation and predrill contingency planning to prevent serious consequences. Ineffective control of the shallow-water flow can result in pressurized sand slurry up the wellbore annulus, leading to sediment build up on the sea bed, washout of the well bore, damage to casing, re-entry problems, and costly

delays in the drilling program (Opseth et al., 2009). A highly cost-effective approach to soft water flow mitigration is simply to avoid or minimize soft water flow risks in the selection of drill site after geohazard evaulation. Judd and Hovland (2009) suggest that this has been the preferred solution in the Golf of Mexico.

3.3 Shallow gas

Davis (1992) define gas-charged sediments down to 1000 m below seabed as shallow gas. Shallow gas constitute a significant blowout hazard during drilling operation (Sills and Wheeler, 1992). Shallow gas-charged sediments can be found in a wide range of depositional settings. If sealed by impermeable fault or sediments, the zone might develop a pressure buildup in gas given lack of chimney to provide a release, potentially leading to a consequent blowout. In parts of North Sea shallow gas charged iceberg plow marks has proven to be a significant drilling hazard (Chopra and Marfurt, 2007, Ch. 14). The formation of plow mark results from winds and currents moving icebergs, dragging the keels along seabed. The plow marks may then be filled with new sediments before buried and sealed, and risk being charged with migrating gas and become over-pressurized.

Szabó (2001) express two common situations for the shallow gas hazard in the drilling operation. The first is gas encountered at shallow depths for which the formation fracture gradients are low, limiting the pressure control using conventional shut-in techniques, at depths ranging from sea bed to casing setting point in conductor or surface casing operations. The other comprise blowouts occurring in open hole below conductor or surface casing. The flow cannot be closed-in and killed with conventional techniques. However, the shallow gas does not only constitute a blowout risk, but also may lead to sudden introduction of gas into the water column. This will cause a decrease in the density of the water-gas mixture which could collapse the platform or sink the drill ship, effectively illustrating the significance of shallow gas assessment in the geohazard studies. Haavik and Landrø (2014) list additional motivations for the identification of shallow gas in the exploration and production of hydrocarbons, including the recognition of shallow gas among indicators of a working petroleum system in region.

3.4 Geohazards on the Norwegian continental shelf

In 1996 the Statoil operated Troll A-platform was towed into the North Sea, and placed at 300 m depth. Geophysical surveys was performed at platform site before installation, but the assessment did not identify the presence of any considerable geohazard risk. Nearly ten years later large amounts of gas was proved to accumulate in and around the platform foundations. Further surveying determined increased sediment temperatures, resulting from operation of the production wells, was leading to thermal expansion of previously unidentifiable gas. To address this hazard, engineers installed venting modifications to

the Troll A foundation systems. These modifications were successful, and the platform continues operation to this day (Brothers et al., 2010).

The Troll A-example is an illustrating example of the three-step approach the oil & gas industry follows on the Norwegian continental shelf to assess geohazards: identification, prevention and mitigation. The initial identification comprises identifying geohazard zones prior to drilling, while prevention is the evaluated well site selection and drilling planning. Thus, mitigation is consequently the remediation of geohazard drilling problems once these are encountered (Dutta et al., 2010). On the Norwegian continental shelf geohazard risk assessment should be conducted in accordance with NORSOK Standard Z-013 - Risk and Emergency Preparedness Analysis, as illustrated by a suggested workflow in **Fig. 3.2** (NORSOK Z-013, 2010). The NORSOK standard introduce requirements to initial planning, operation and use of risk analyses associated with exploration, production and transport of hydrocarbons as well as all fixed and moving assets comprised by the activity.

3.5 Geohazard surveying technology

Dedicated geophysical tools used to help characterize offshore sites and asses geohazards include side-scan sonar and multi-beam systems, subbottom profilers and multichannel seismic data. They differ greatly with regards to output data resolution, penetration depth, operating cost and efficiency, and the choice of technology for a survey should hence be governed by the target of the investigation, project size and economy, plus available market supply.

The side-scan sonar is an acoustic device imaging the seabed in 2 dimensions with near photographic quality. The side-scan sonar system is towed behind the vessel and emit frequencies in the range of 100 Hz to over 1 MHz. More commonly, side scan systems used for shallow water geosurveys work with frequencies between 50 kHz and 500 kHz. The multi-beam sonar utilizes beam forming, using two source arrays, a source array whose long axis is parallel to the direction of travel and a perpendicular receiver array, each emitting a narrow, fan-shaped beam (Plets et al., 2013).

Sub-buttom profiling systems include boomer, sparker, pinger and chirper systems and are often configured much like conventional seismic air gun acquisition. Pinger and chirp systems operate at frequencies between 2 and 12 kHz, with source and hydrophones configured in one unit towed or mounted over the side of the vessel. They are capable of penetrating up to 60 m below sea bed in ideal conditions. Boomers and sparkers configure source and receivers separately and may consequently deliver greater power output without damages. Boomers operate in the frequency range of 500Hz to approximately 4kHz, and sparkers about 200Hz to 800Hz and may therefore image greater depths than pinger and chirpers, but compromise the resolution.

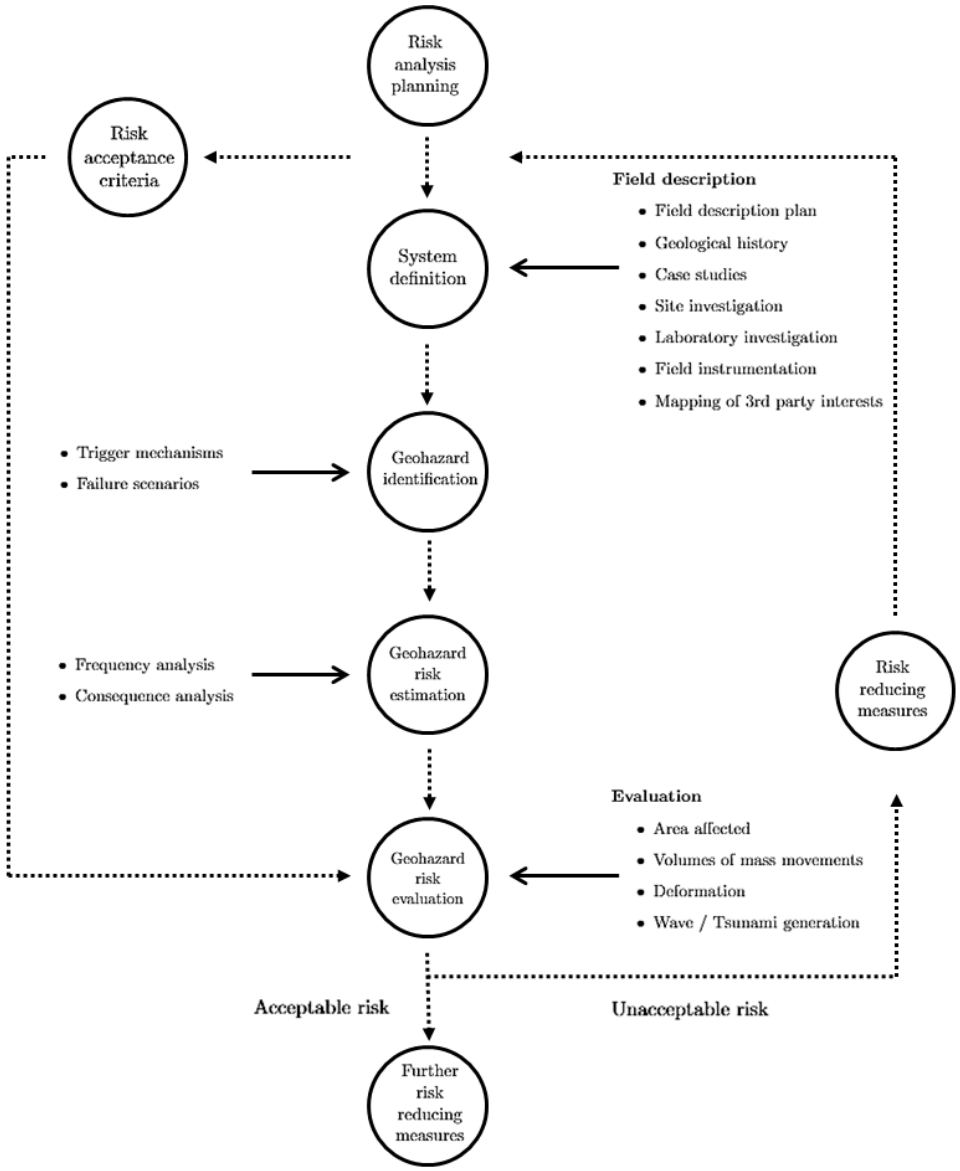

Figure 3.2 – *Offshore geohazard risk assessment process, based on NORSOK Z-013 (Figure modified after NGI (2005))*

3.6 3D exploration seismic data in geohazard assessment

Conventional 3D exploration seismic data is currently experiencing increased attention in geohazard assessments by the oil & gas industry (Farouki and Sakamoto, 2013). Seismic streamer data is already key input to the planning and execution of successful exploration campaigns by using the seismic depth image and its estimated parameters such as pore pressure fracture gradients and geomechanical properties. Economical and logistical rationality suggest that utilizing the already acquired seismic data for the geohazard assessment would be a cost-effective approach to resource management for the explorationists. Already in the late 90's Campbell (1999) suggested that successful implementation of 3D exploration seismic data should be the most reliable approach to minimize risk in a preliminary geohazard assessment. However, narrow bandwidth strongly restraining resolution has historically limited the use of conventional seismic data for this use.

Dutta et al. (2010) compare the targeted site survey data with exploration seismic data. The site survey data has the superior temporal and spatial resolution over the acquired area, and can hence be used in detailed stratigraphic and bathymetric interpretation. The geohazard survey data does, however, require the actual extra acquisition at a cost, and has short or no offset recordings. The latter strongly limits quantitative assessment techniques such as inversion and AVO-analysis. 3D exploration seismic, on the other hand, is typically readily available for assessment and has large offsets. However, the signal to noise ratio is often sub-par for a detailed stratigraphic interpretation and the frequency bandwidth does not yield the high resolution a site surveys may offer. For new exploration surveys technological developments, including broadband solutions, will oppose some of this challenges and better prepare the data for a geohazard study. For the already acquired data targeted reprocessing has shown great potential for geohazard preparation with the enhanced denoising and deghosting techniques offered by the processing contractors. Several recent publications have discussed successful approaches and techniques for the use of both newly acquired and reprocessed 3D seismic data in near surface geohazard assessments (Farouki and Sakamoto, 2013; Sharp and Badalini, 2013; Farouki et al., 2012), including the prediction of shallow water flow Dutta et al. (2010), fault investigation (Ebuna et al., 2013) and shallow gas detection (Toxopeus et al., 2011). With the assumption that broadband technology is likely to become industry standard in both acquisition and processing systems we should expect to see more seismic data in geohazard studies in the future.

Chapter 4

3D broadband processing of North Sea case study

4.1 The 2/4-14-blowout

The study area is located in Central North sea, block 2/4. In 1989 the area experienced a major underground blowout when Saga Treasure drilled wild-cat well 2/4-14 into a rotated Jurassic fault block on the Steinbit Terrance, encountering a high pressure zone before ultimately losing control of the operation. The well developed into an underground blowout lasting for 326 days, before it was killed 13th December 1989 (Landrø, 2011). Remen (1991) estimates 0.4 million m^3 of oil and 196-367 million m^3 of gas migrated from the reservoir into shallow formations before the blow out was killed using a relief well. Main recipients for the hydrocarbons are suggested to be thin sand layers at approximately 490 meters and 840 meters below mean sea level. Saga Petroleum initiated a dedicated time lapse acquisition campaign with surveys 4, 6, 10 and 48 months after the blow out to facilitate the development. This data has provided useful information on the migration of the gas. For further reading on the 2/4-14 blowout reader is advised to Landrø (2011)

The 3D seismic dataset used for this case study is SG9111 acquired by Geco-Prakla for Saga Petroleum during the period 1. March , 1991 to 28. July, 1991, using vessel M/V Geco Echo configured with dual source and dual streamer. Acquisition parameters are listed in Table 4.1. In an earlier study Landrø (2011) produced simple time lapse difference stacks using 2D lines showing clear anomalies in the gas recipients. By using best practice commercial processing technology this broadband processing workflow will specifically target these shallow gas recipients to open up for new quantitative 3D studies.

LOSEM1991	
Source depth	7 m
Streamer depth	9 m
Group interval	12,5 m
Number of cables	2
Source separation	50 m
Streamer separation	100 m
Shot point interval	25 m, flip to flop
Traces per cable	272
Sample rate	2 ms
High-cut acq. filter	125 Hz
Lo-cut acq. filter	3 Hz
Minimum offset	205 m
Nominal fold	60

Table 4.1 – *LOSEM1991 acquisition parameters*

4.2 Broadband processing workflow

The avaliable data provided include 154 sail lines, observers log and the final acquisition report delivered to Saga Petroleum. The acquired lines fully cover the well, as imaged in **Fig. 4.1**. The survey is gridded with origo $(X, Y) = (510233.3442, 6251652.71645)$ real world coordinates and rotation 55 degrees off north. Bin size is 12.5 m in crossline direction and 37.5 m in inline direction.

Also available for processing is a velocity model built for QUAD 30 phase V / NQ8, a 2005 CGG Multiclient survey over the same area. The velocity model was extracted, interpolated to infill missing data and cropped to fit the seismic volume.

The raw data hold decent quality, at least considering its vintage. Raw shot gathers display clear primary recordings and medium noise level at shallow parts, except for some pronounced linear noise throughout the data as seen in **Fig. 4.2** The frequency spectrum is also encouraging, suggesting potentially recoverable signal up to about 80-90 Hz. Full trace length is 8 seconds, but the shallow gas of interest is expected at $< 1s$ meaning less attention will be divided to deep recording noise artifacts seen in the gathers, as data is cut at 4 seconds length early in the workflow. **Fig. 4.3** shows a common receiver gather brute stack for quality check of a raw subline. The stack shows pronouced amplitudes at the expected shallow gas layers and its multiples. The filter panel in **Fig. 4.4** indicate presence of parimary signal even at the higher frequencies, potentially allowing for a broader frequency band by deghosting and denoising.

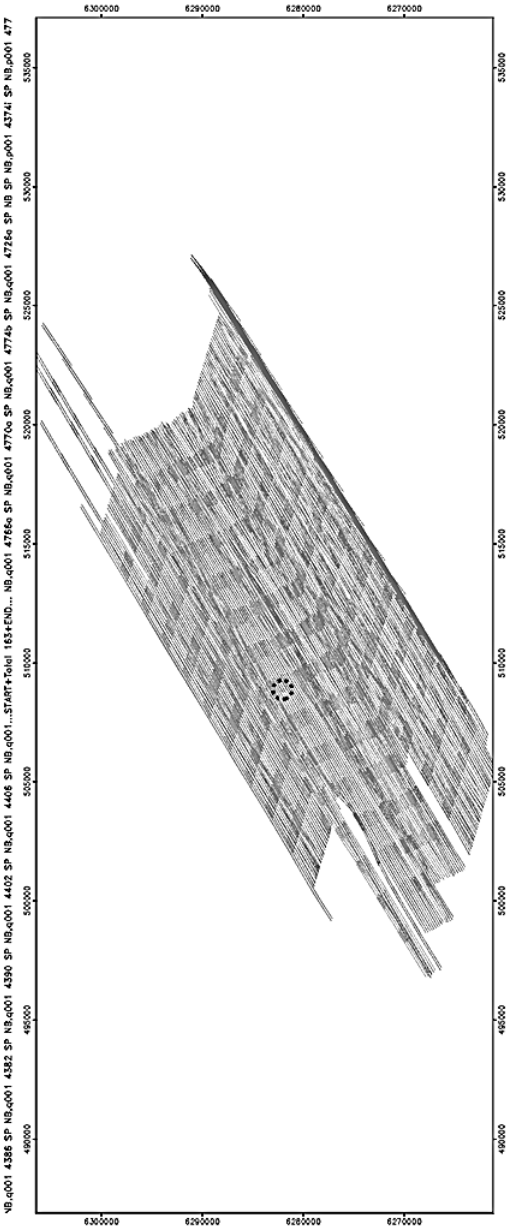

Figure 4.1 – *SG9111 - Survey mapview with well loction marked by dottede circle. Axis note real world coordinates.*

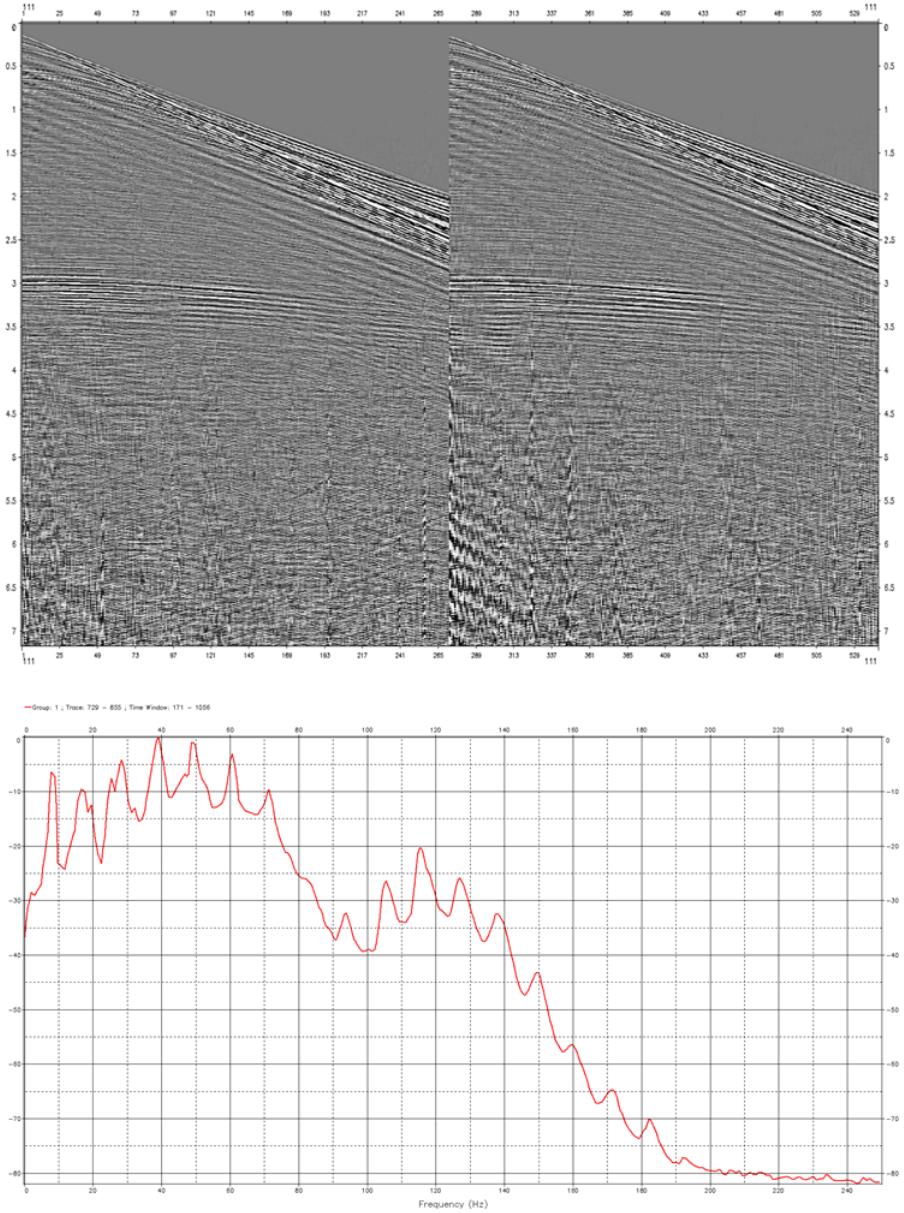

Figure 4.2 – *Raw shot, Sail line 4506. Top: Raw shot gather, both cables, 0-8 s traces. Bottom: Amplitude spectrum. Amplitude in dB from 0 to -80. Frequencies from 0 to 250 Hz.*

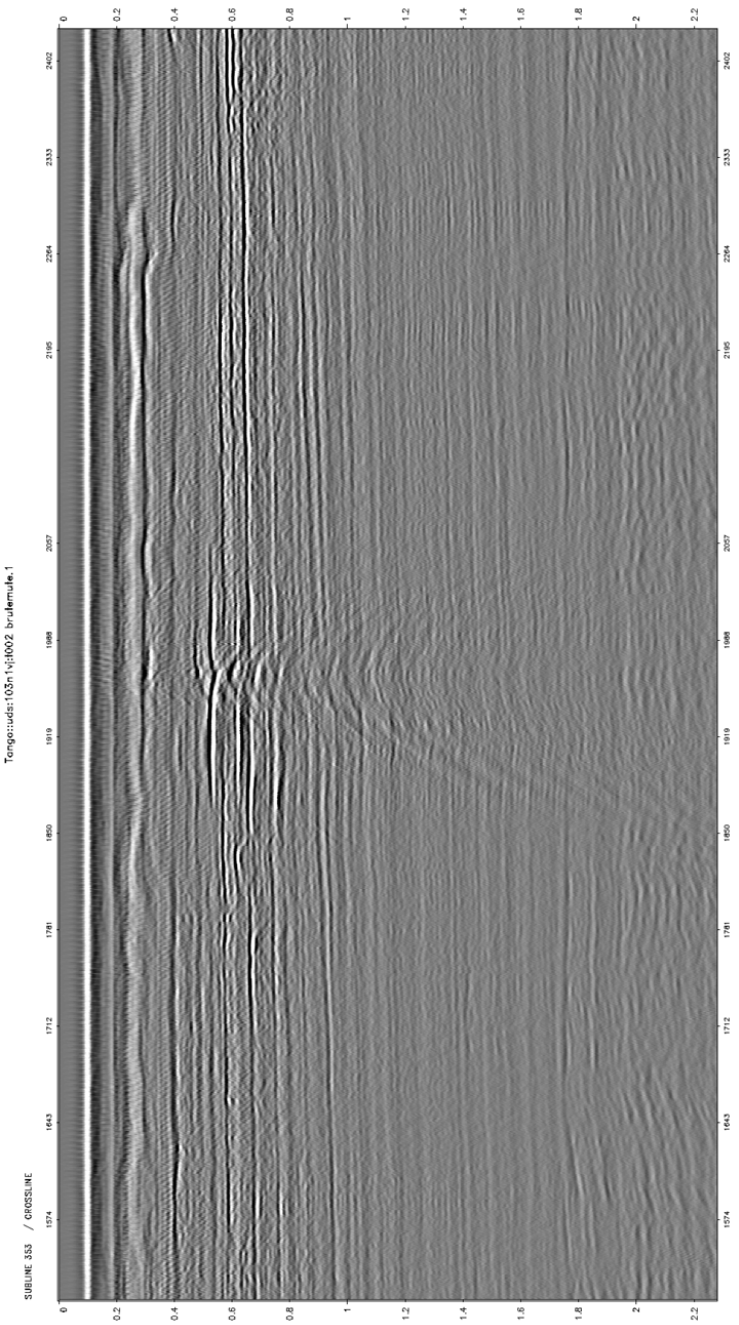

Figure 4.3 – *Brute stack - Sail line 4506. Common receiver gather centered near well location. Note the diffraction hyperbolas around gas recipient layer edges. 1 cable, 1 gun, 0-2.2 s. window*

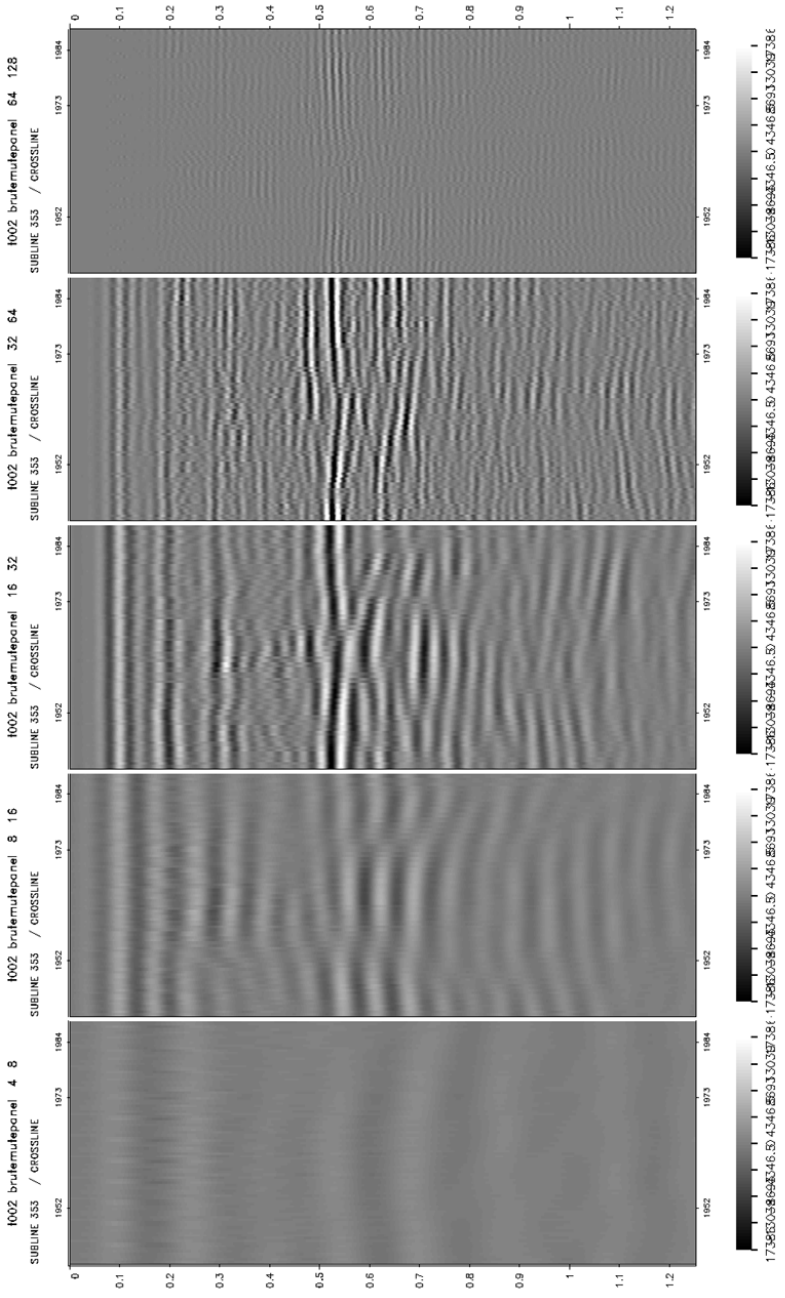

Figure 4.4 – *Brute stack filter panels - Sail line 4506 centered arond well location. From left to right: 4-8 Hz, 8-16 Hz, 16-32 Hz, 32-64 Hz, 64-128 Hz. 1 cable/1 gun, 0-1.25 window*

The data is prepared for processing by applying necessary attributes and setting a psuedo 2D geometry on the recordings performed by creating sublines with unique identity for each gun/cable combination possible. For a 2-gun-2-cable configuration this yields 4 sublines, allowing convenient subline sorting on 1-gun-1-cable through the workflow.

4.2.1 Designature

The designature was preformed using a modelled signature as described in Ch. 2.5.1, producing a zero-phase wavelet and flattening the spectrum by targeting the source ghost. The receiver ghost however is preserved for the dedicated deghosting operator later in the workflow.

Testing

The final acquisition report provided by the LOSEM consortium state information on the recording parameters for the signature model input. The acquisition was performed using Nessie II recording instruments, at 6 m depth, with low-cut filter at 3 Hz with 18 Db per octave slope and a hi-cut filter at 125 Hz with 72 Db per octave slope. The options available in modelling software however could only provide for the option of a Nessie 3.3 recording instrument model with a low-cut filter 3.3 Hz with 18 dB per octave slope and high-cut filter 125 Hz with 70 dB per octave slope *or* DFS-V recording instrument model and a low cut filter 3.5 Hz with 18 dB per octave slope and high-cut filter at 128 Hz with 72 dB per octave slope. Both options was tested in the designature yielding subpar results as shown in **Fig. 4.5**. By investigating the modelled signature it is evident that the configuration is not successfully reproduced by the modelling settings. Both signatures contain an unrealistically strong bubble, and the designatured gathers are heavily smeared. This may be explained due to the vintage of the acquisition equipment accounting that potentially lacks support in the commercial processing algorithm.

To mitigate, a custom designature was created using depth and gun chamber volume configuration only. This effectively results in complete preservation of the bubble until a designated debubble operator is applied at later stage if appropriate. The custom signature is convolved with the wavefield to yield source ghost free data as illustrated in **Fig. 4.7** and **Fig. 4.8**.

Some frequencies in the 80-100 hz range has been sucessfully recovered. However, from the shot gathers in **Fig. 4.7** it is evident that out convolution operator boost the linear noise.

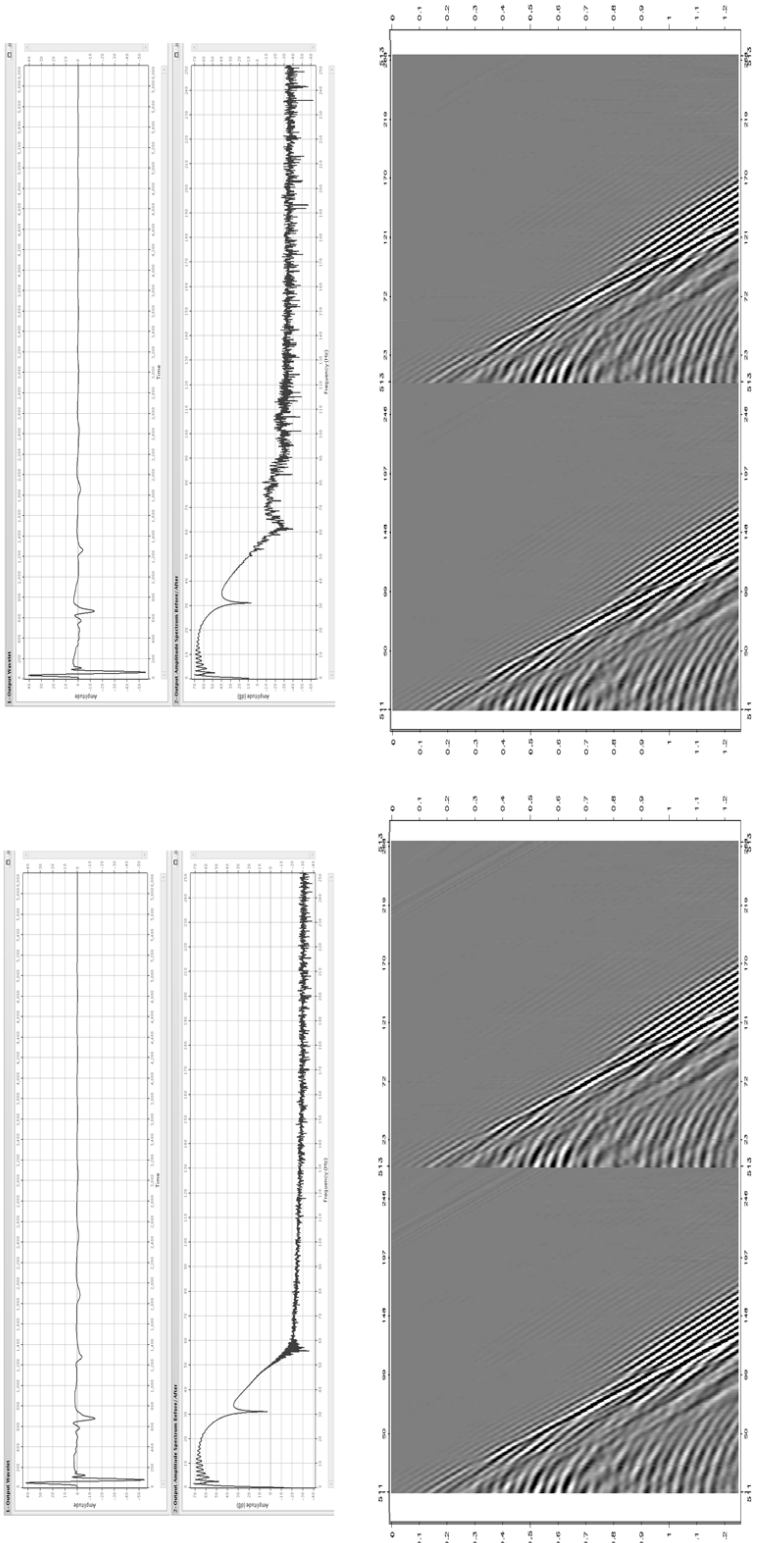

Figure 4.5 – *Designatured shot gather and amplitude spectrum - Algorithm modelling test. Left: Nessie 3.3 configuration. Right: DFS-V configuration. Top: Signature and amplitude spectrum. In dB from -50 to 40 and in ms from 0 to 6000. Bottom: designatured shot gather, 2 cables, 0-1.2 s window.*

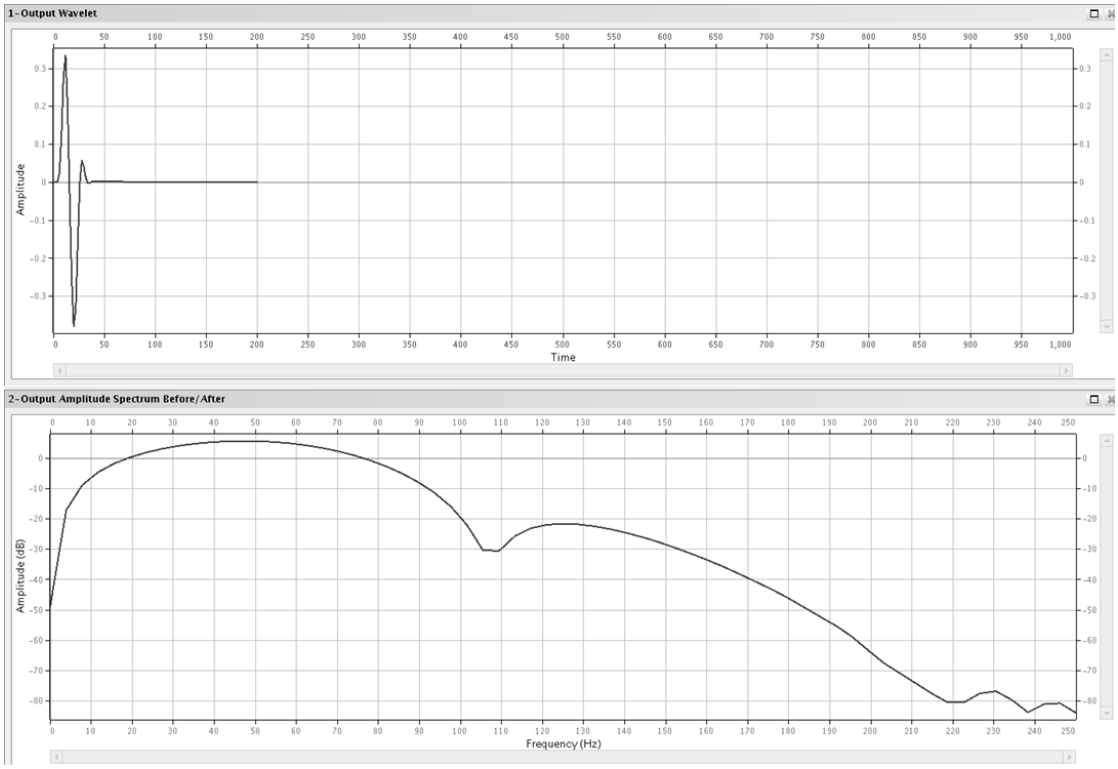

Figure 4.6 – *Custom signature model with source ghost only. Top: Signature. In ms from 0 to 1000. Bottom: Amplitude spectrum. In dB from 0 to -80, Hz from 0-250*

4.2.2 Linear noise attenuation

The physical origin of the linear noise patterns has been considered but not concluded. Discussions with processors suggest that similar noise patterns are trending in several old Geco-Pracla acquisitions from this vintage, and might emerge from the original receiver systems at the vessels. The frequency spectrum indicate that the noise is in the $< 10Hz$ range.

Testing

Regardless of origin, the strong linear noise dominate the shot gathers after further boosting by the designature convolution. To mitigate the linear noise a K-filter followed by a Radon filter is utilized. The K-filter designs and applies a spatial low pass filter specified in fractions of K-Nyquist attenuating wavenumbers above the set fraction.

After the K-filter a constrained, high resolution, linear Radon transform is applied, designed to produce a sparse set of events in the transform domain. The strength of

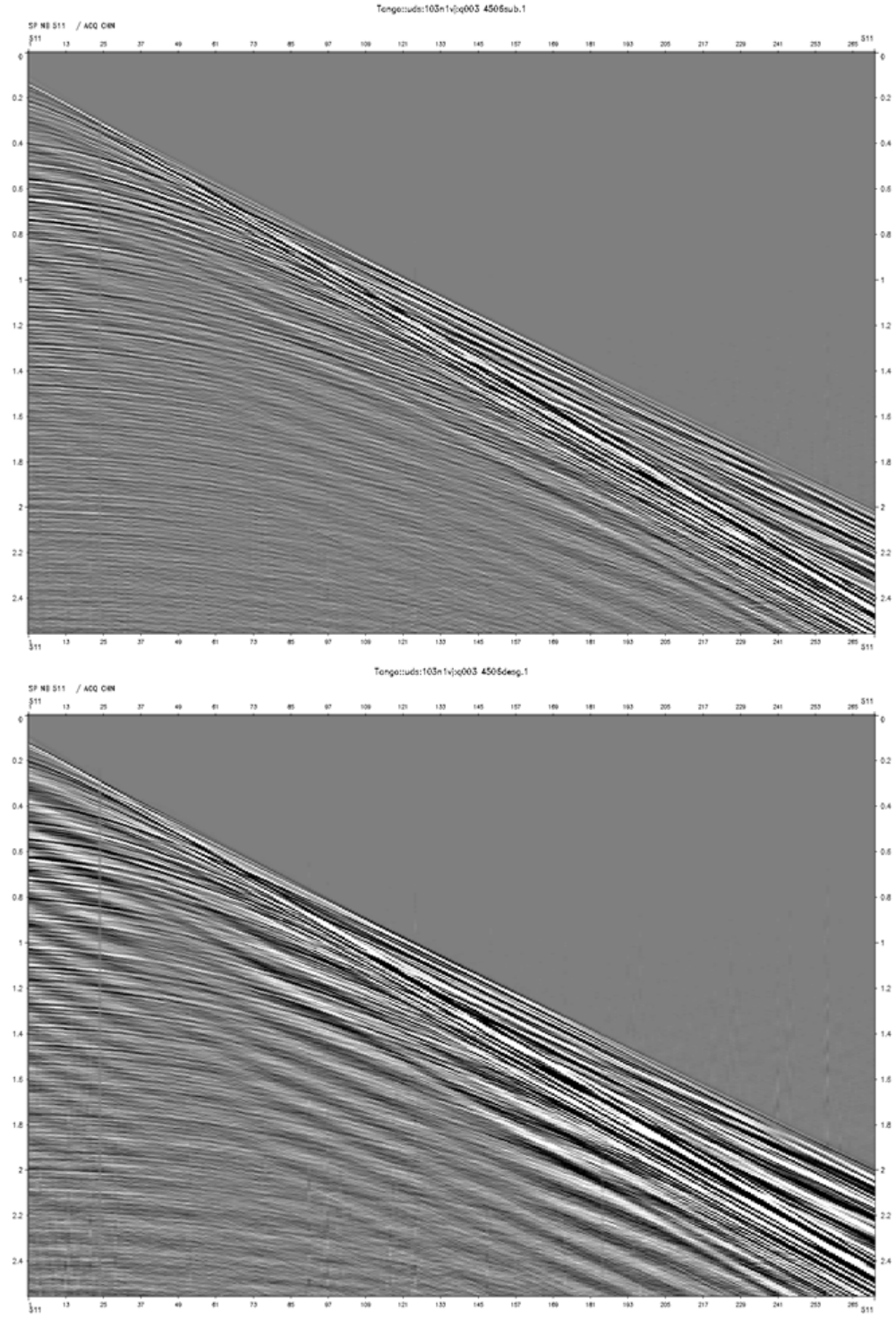

Figure 4.7 – *Top: Raw shot gather. Bottom: Designatured shot gather. 1 shot/1 cable, 0-2.5 s window.*

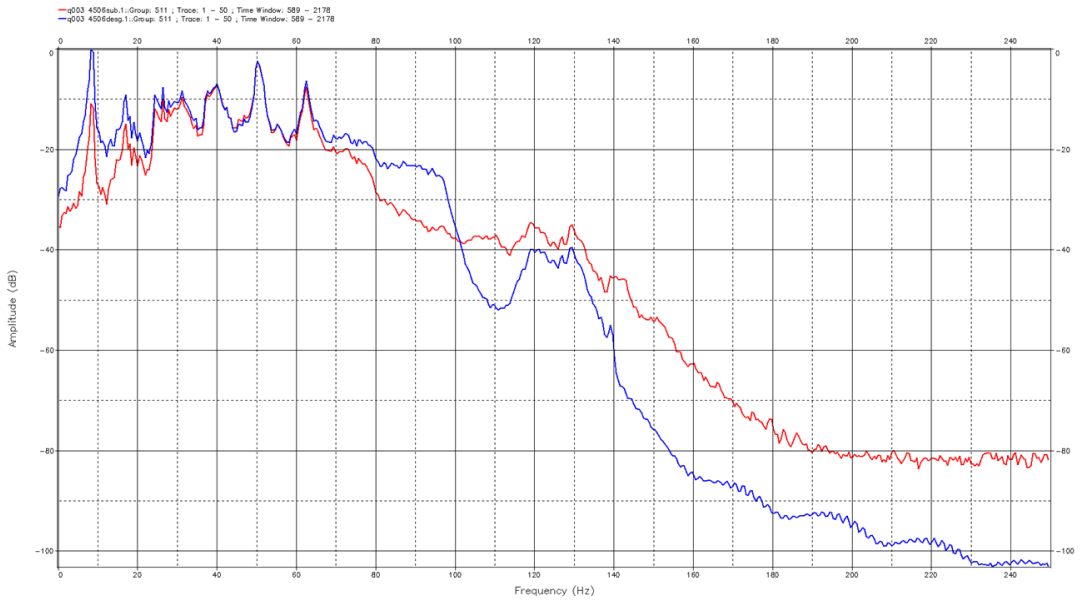

Figure 4.8 – *Amplitude spectrum of shot gather. Red: Before designature. Blue: After designature. Amplitude in dB from 0 to -100. Frequency in Hz from 0 to 250. All data 1 shot/1 cable, 0-4 s window.*

the constraints and the sparsity of events are controlled by tested input parameters to reduce smearing and aliasing in Radon domain. The result of the forward transform is divided into two separate dip ranges, one of which represents signal and the other noise. A frequency domain signal model and a similar noise model are generated by inverse transformation back to original domain to produce a noise free-output.

Upper and lower limit of the dip values used to represent all events in data are tested along lowest and highest frequency allowed to represent data in the Radon domain. Dip range low -2000 μs / high 1000 μs is tested versus -1000 μs / high 500 μs. Frequency dependency range 10-80 Hz is tested versus 0-100 Hz. The test is shown in **Fig. 4.9**.

The testing suggest the broadest frequency range yield better results. The required computational power is greater for broader band, but the noise attenuation is superior. The dip range variation tested, however, seems to only affect the attenuation to a limited degree, and the broader dip range is preferred to prevent exclusion of data. Parameter combination 0-100 Hz, -2000 - 1000 μs is applied to the production. Results are shown in **Fig. 4.10**.

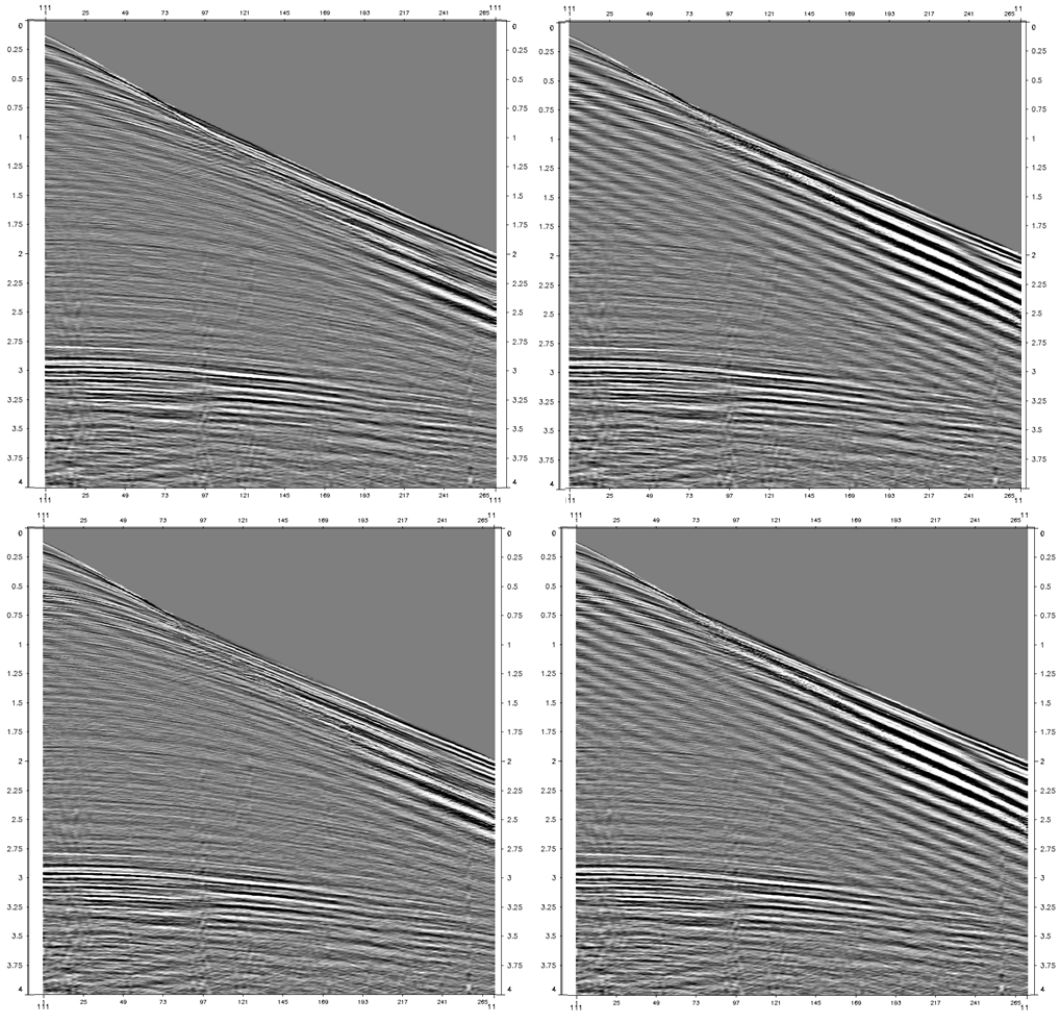

Figure 4.9 – *Denoised shot gather - Dip range and frequency test. Upper left: 0-100 Hz, -2000 - 1000 µs. Upper Right: 10-80 Hz, -2000 - 1000 µs. Lower left: 0-100 Hz, -1000 - 500 µs. Lower right: 10-80 Hz, -1000 - 500 µs. All gathers are 1 shot/1 cable, 0-4 seconds window*

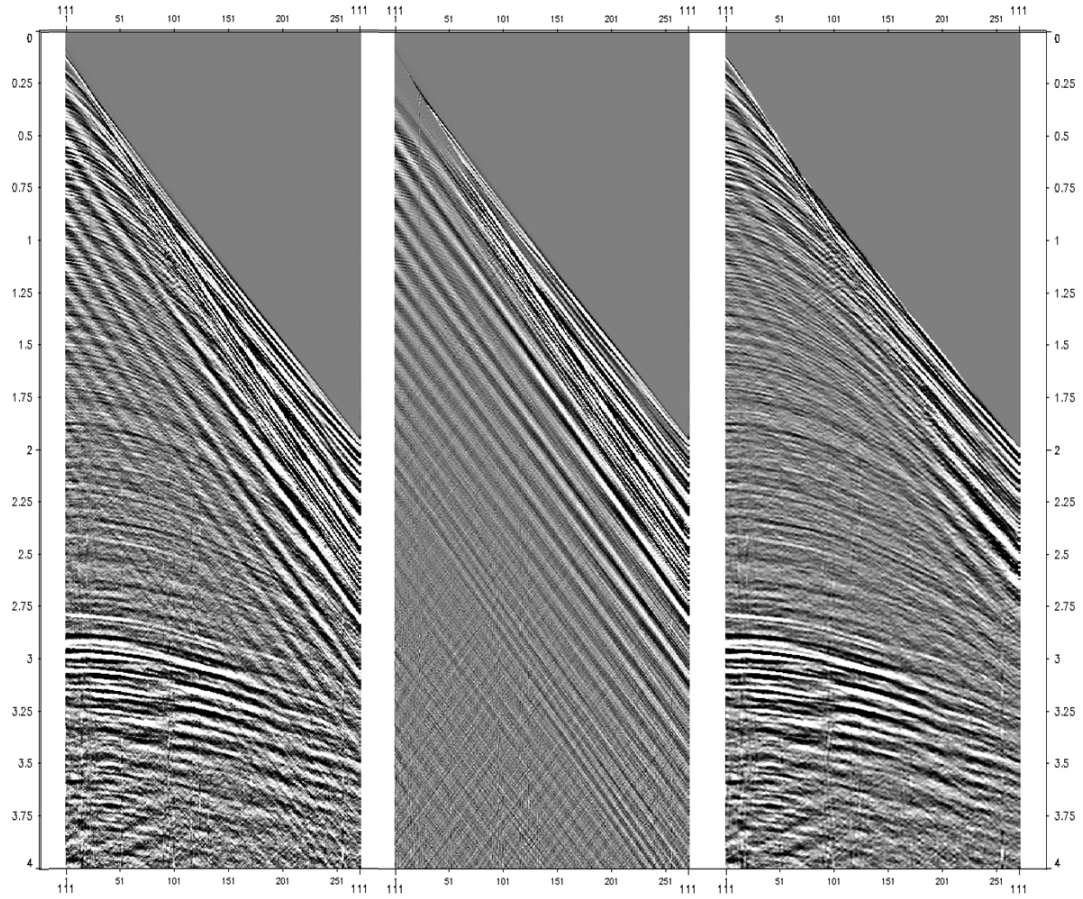

Figure 4.10 – *Linear noise attenuated shot gather. Left: Input data. Mid: Noise model. Right: Linear noise attenuated output data, input data subtracted noise model. All gathers are 1 shot/1 cable, 0-4 seconds window*

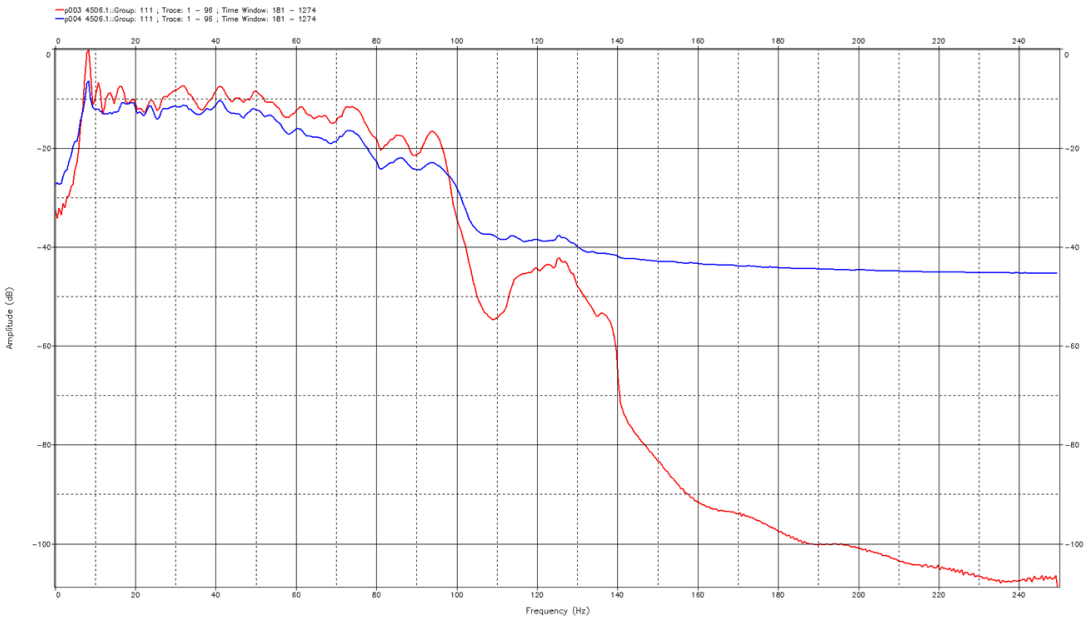

Figure 4.11 – *Denoised shot amplitude spectrum. Red: Before denoising. Blue: After denoising. Amplitude in dB from 0 to -110. Frequency in Hz from 0 to 250.*

4.2.3 Deghosting

To mitigate the receiver ghost, Gordon Pooles pre-migration receiver deghosting algorithm is applied. The technique derives a surface datum ghost free model of input seismic data useing least squares linear Radon equations (Poole, 2013).

Testing

The algorithm has proved to be very robust, and is preferred over Wang and Peng (2012)'s bootstrap technique in this workflow due to convenient implementation. The operator essentially inputs the acquisition configuration only, including the receiver spacing and depth, hence requiring limited parameter testing.

Evaluation of the shot gathers before and after deghosting in **Fig. 4.12** reviles successful application. Assumed that the input data can be considered the processed recording of a combination of the up- and downgoing wavefield in the water column as discussed in Ch. 2.4, successfully deghosted data should contain upward wavefield recordings only. The subtraction of deghosted data minus original data should there theoretically yield the ghost data only (with reversed polarity), as observable in **Fig. 4.12**. The results in **Fig. 4.13** also suggest encouraging deghosting, but some reduction in signal strength seen in the amplitude spectrum.

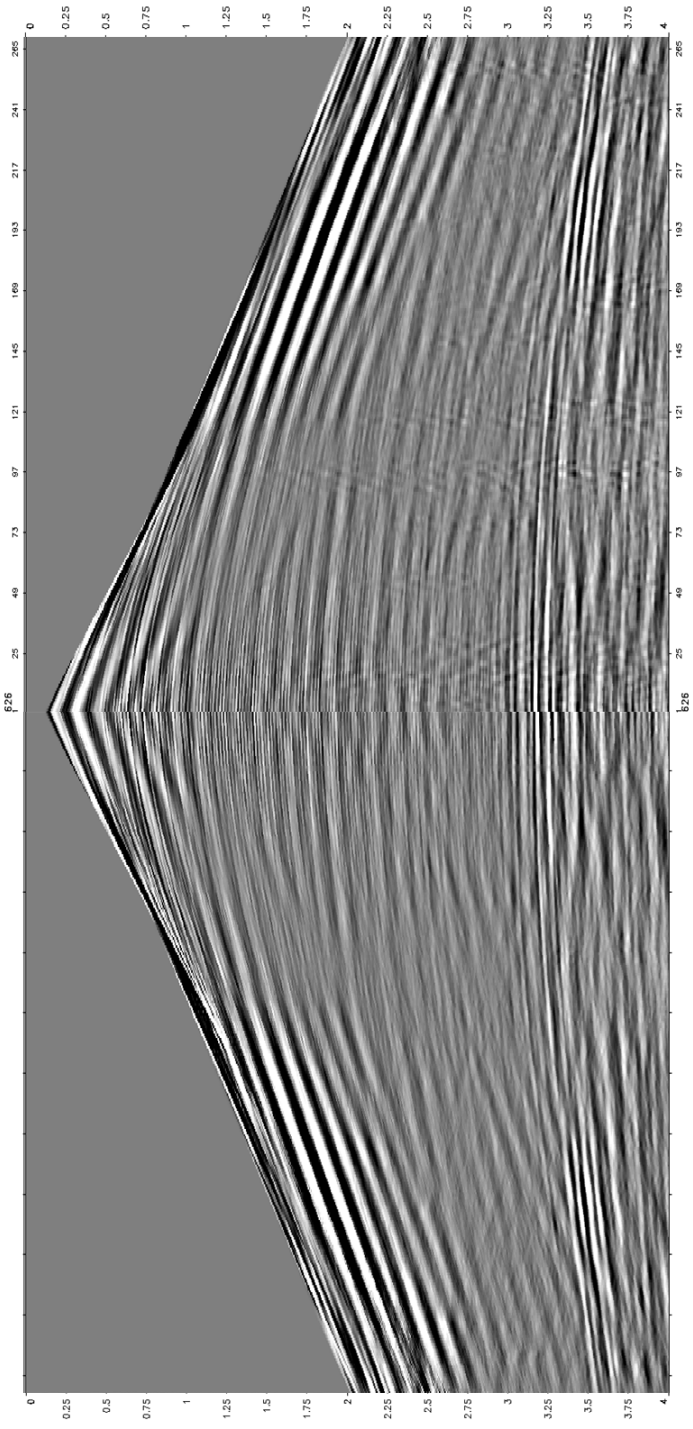

Figure 4.12 – *Deghosted and deghosted subtracted ghosted shot gather back to back Left: Deghosted subctracted ghosted shot gather. Right: Deghosted shot gather. 1 shot/1 cable, 0-4 seconds window.*

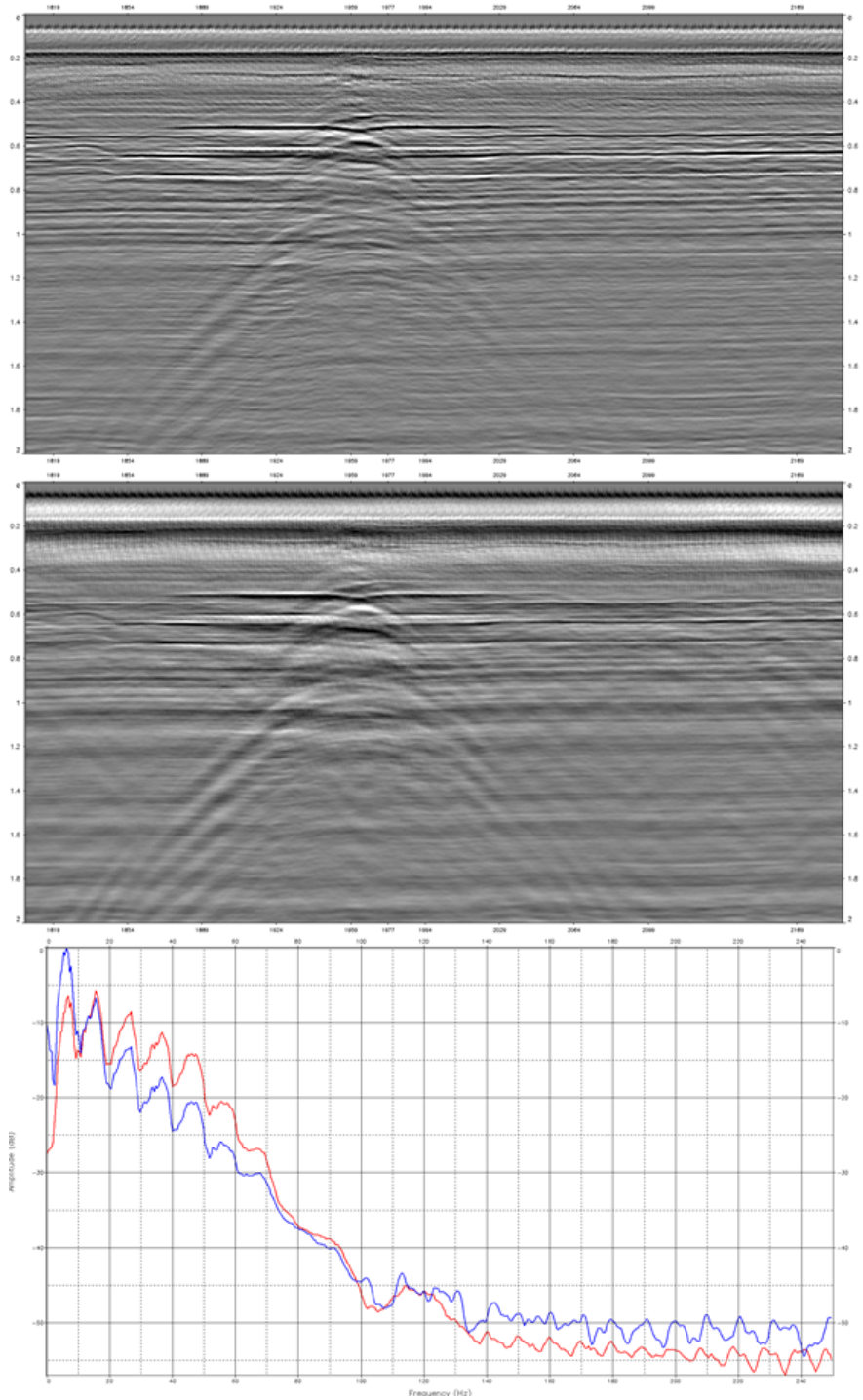

Figure 4.13 – *Deghosted and deghosted stack from - line 4506. Top: Ghosted stack. Mid: Deghosted stack. 1 shot/1 cable, 0-2 seconds window. Bottom: Amplitude spectrum. Red: Before deghosting. Blue: After deghosting. In dB from 0 to -95 and Hz from 0-250.*

4.2.4 Demultiple

Multiples are present throughout the data, and can be seen in both stacks and gathers. To mitigate, a gap deconvolution demultiple operator in tau-p domain is applied to the successfully deghosted gathers. The demultiple operator seek to identify the primary reflection series by considering the model of a trace as a convolution of random spikes with minimum phase wavelet and additive noise. The special gap deconvolution operator is consequently directed to reverberations which have delays equal to, or greater than, the prediction gap delay parameter set as input. By using a running average technique the algorithm computes an average autocorrelation for each trace accomplished by adding the autocorrelations over an offset range equally spread on either side of that trace.

Testing

The autocorrelation active filter and gap parameters is to be set long enough to include of the targeted multiple information. For this dataset parameter testing was performed for 3 active filter and gap length combinations: 40 ms filter length / 60 ms gap length, 80 ms filter length / 220 ms gap length, and 60 ms filter length / 40 ms gap length, as shown on frequency spectrum in **Fig. 4.15** and on shot gathers in **Fig. 4.14**. The comparison suggest the 40 ms filter length / 60 ms gap length and 60 ms filter length / 40 ms gap length have the most encouraging results. The latter noise model, however, may seem to include some components of the primary reflection series. By evaluating the amplitude spectrum we also see that we do recover frequencies in the top end of the band for both combinations.

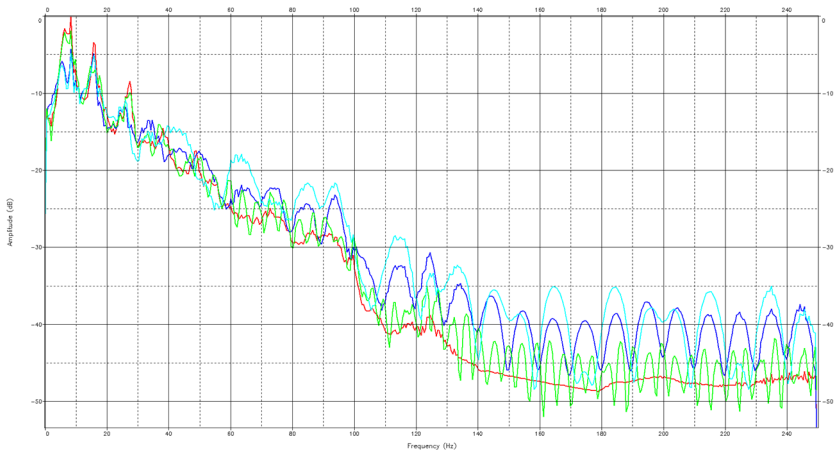

Figure 4.14 – *Demultipled shot gather - Filter and gap length test. Red: Original gather. Blue: 40 ms filter length / 60 ms gap length. Green: 80 ms filter length / 220 ms gap length. Turquoise: 60 ms filter length / 40 ms gap length. In dB from 0 to -55 and Hz from 0 to 250.*

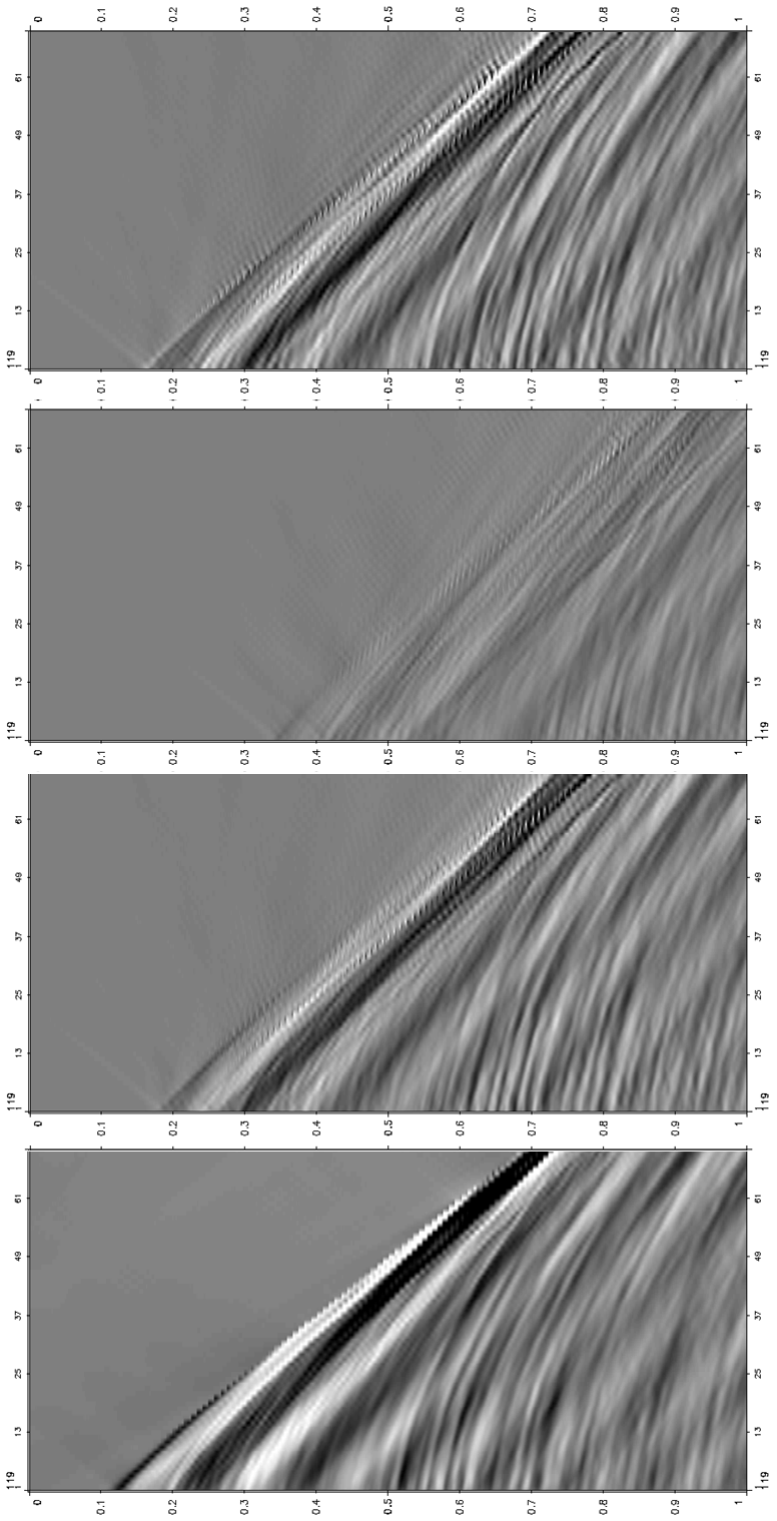

Figure 4.15 – *Demultipled shot gather noise model - Filter and gap length test. Left: Original gather. Left mid: 40 ms filter length / 60 ms gap length multiple model. Right mid: 80 ms filter length / 220 ms gap length multiple model. Right: 60 ms filter length / 40 ms gap length multiple model. All data 1shot/1 cable, 0-1 s window.*

Production results for active filter length to 40 ms, with a 60 ms gap length, adding up to a total of 100 ms operator length for the deconvolution are shown in tau-p domain in **Fig. 4.16** and on shot gathers in **Fig. 4.17**.

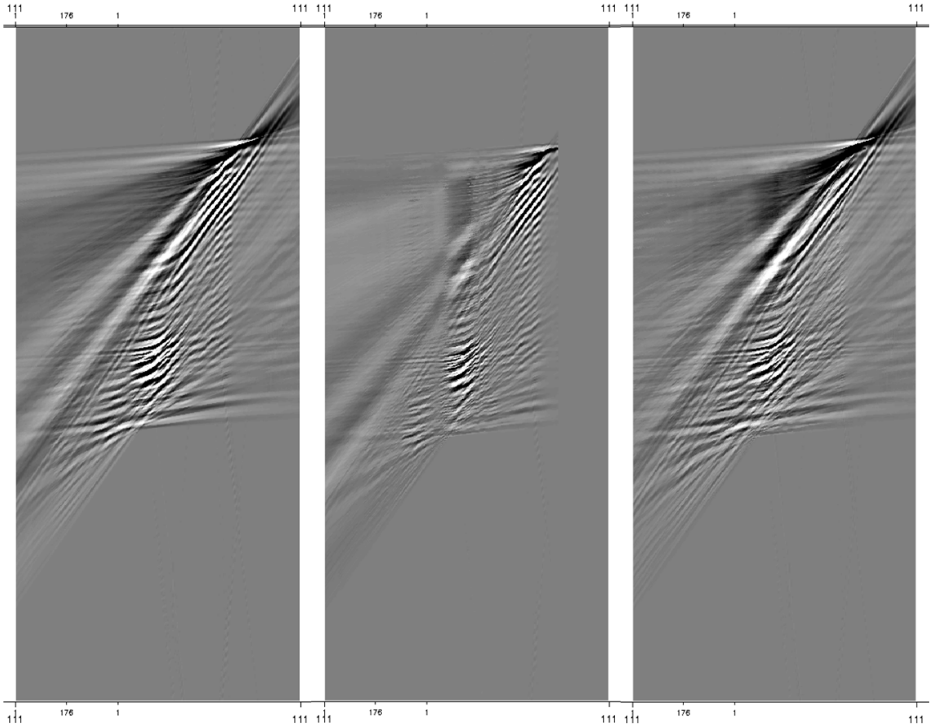

Figure 4.16 – *Demultiple shot gather in tau-p domain. Left: Input data. Mid: Gap deconvolution multiple model. Left: Demultipled gather, deghosted gather subtracted multiple model. X-axis: Ray parameter p. Y-axis: Time intercept value*

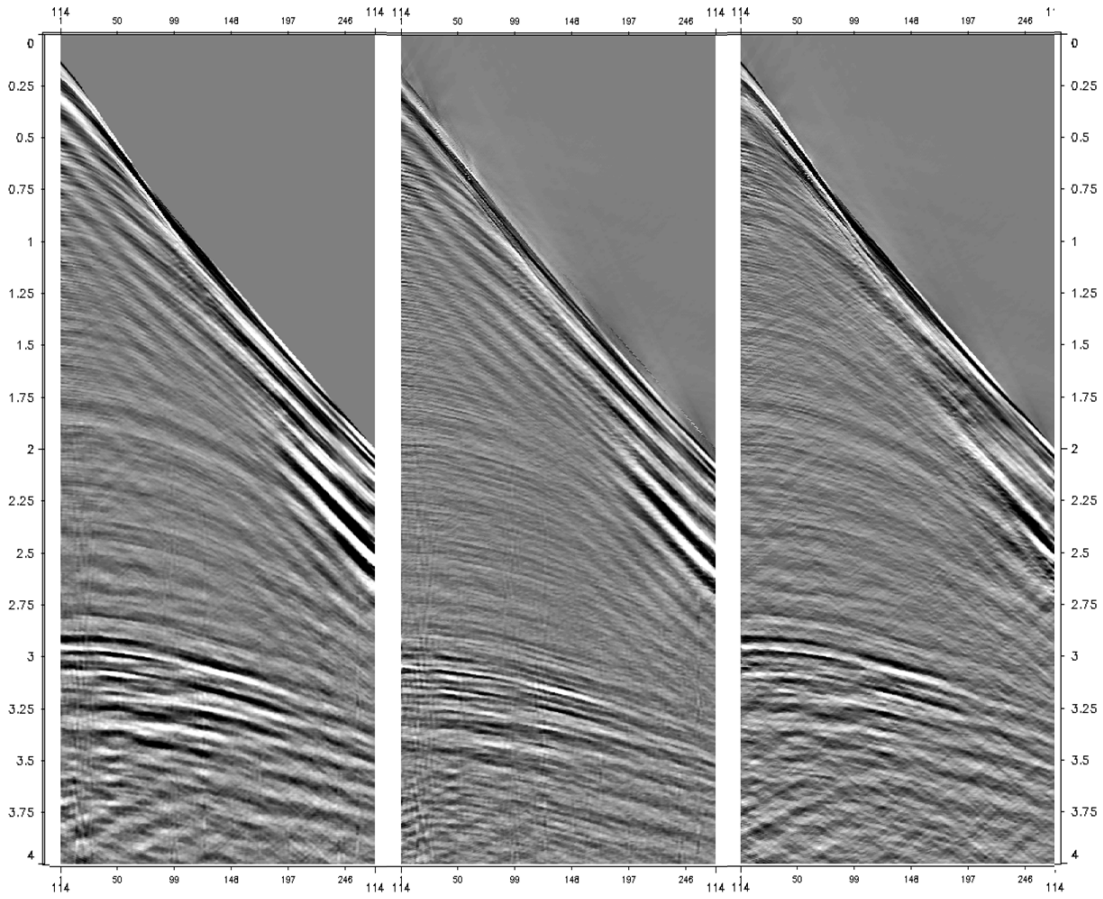

Figure 4.17 – *Demultiple shot gather. Left: Input gather. Mid: Gap deconvolution multiple model. Left: Demultipled gather, input gather subtracted multiple model. All data 1 shot/1 cable, 0-4 s window.*

4.2.5 Binning and regularization

For 3D surveys binning and regularization mark the the end of sail line processing, and the beginning of offset class processing. Binning 3D seismic data is a transformation from survey spatial coordinates into a standardized binning coordinate system. Each bin contain a group of traces related by a common geometrical property, usually that of being close to the same shot - receiver position. During sail line processing the centroid of shot and receiver midpoints are not necessarily at the center of grid cell, implying nonuniform fold, and irregular offset and azimuth distribution per bin. Binning the data assign recordings to common cell gathers defined by the acquisition configuration, here $12,5\,m \times 37,5\,m$, yielding 34 offset classes centred in 224 m - 3424 m offsets with 100 m increment. Binned data in map view is displayed in **Fig. 4.18**

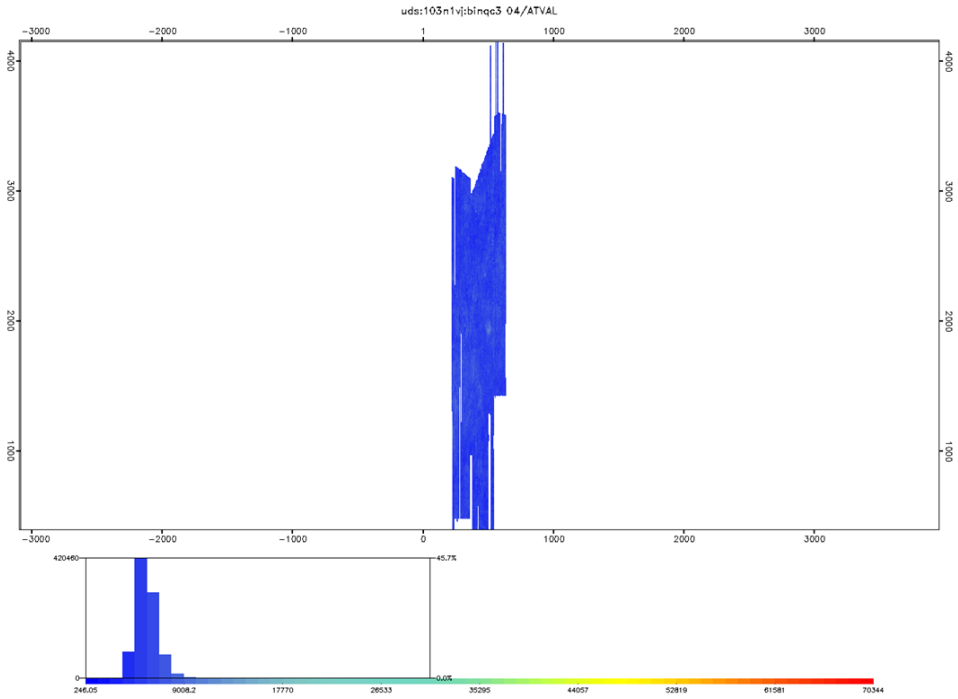

Figure 4.18 – *Survey map view - Binned data for offset class 4/34, centred at 524 m offset. Scale display root mean square values of data over a 500-2000 ms interval. X axis: Inline. Y axis: Crossline.*

The regularization is the centering of traces within their defined bins, and a following fold regularisation, including interpolating missing traces and optional trace duplication. The input data is transformed using an irregular 2D Fourier decomposition applying the input data position. The reverse transform maps the data to the regular grid utilizing an anti alias filter.

4.2.6 Migration

The migration is performed using a Kirchhoff pre-stack time algorithm. The technique is by far the most computational heavy algorithm performed in the workflow, and limited testing was available. The cube cropped to subline 220 to 617 and crossline 1390 to 2160 with 1500 ms cut. Migration aperture is set to 3000 m, while maximum travel time aperture is set greater than maximum offset plus half the migration aperture, hence $>$ 3000 m +1500 m, at 4700m . Travel times are calculated within a maximum horizontal distance of the given parameter value. Global maximum dip in degrees to migrate is set to 70. An anti-alias denoising is preformed by a low pass filtering of input data where the cut off frequency is calculated by the local dip of the summation trajectory. We set spacing of anti-alias filter to CDP spacing $\times$1.5, x-direction to 18.75 m and 56.25 m in y-direction.

Final amplitude spectrum is displayed in **Fig. 4.19**, compared with the raw, unprocessed input data in the beginning of the workflow. Frequencies all over the spectrum have been successfully enhanced by the broadband processing workflow described, and the spectrum is flattened. Selected 2D-images of the results are displayed in **Fig. 4.20**, **Fig. 4.21**, **Fig. 4.22** and **Fig. 4.23**. Both time slices, crossline and subline show clear amplitude anomalies in gashazard on both 520 ms and 650 ms.

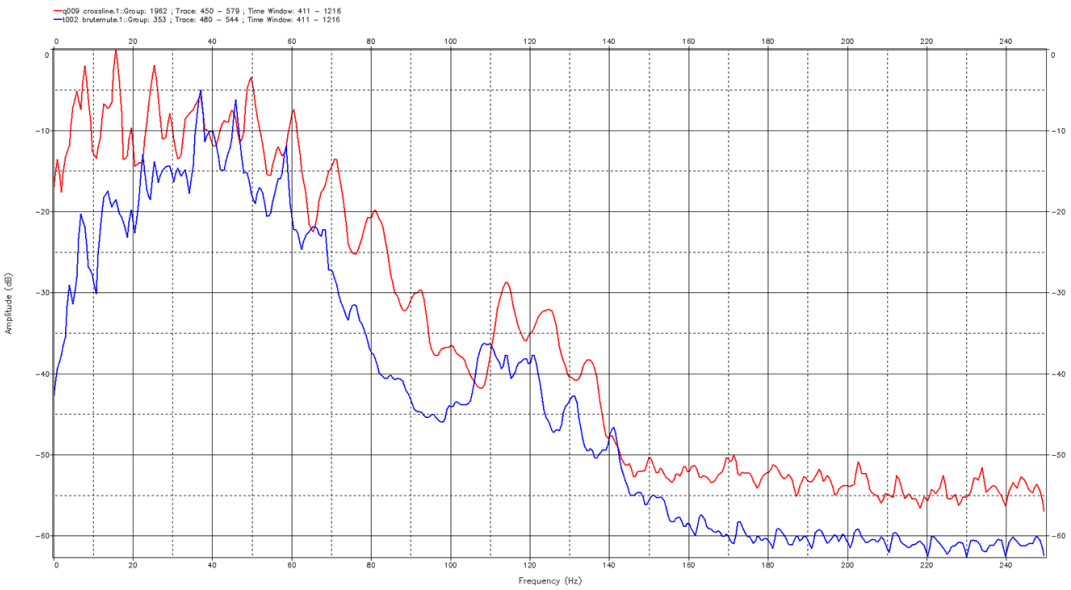

Figure 4.19 – *Migrated cube, offset class 1 - Amplitude spectrum. Blue: Raw subline. Red: Migrated subline. In dB from 0 to -60 and Hz from 0-250.*

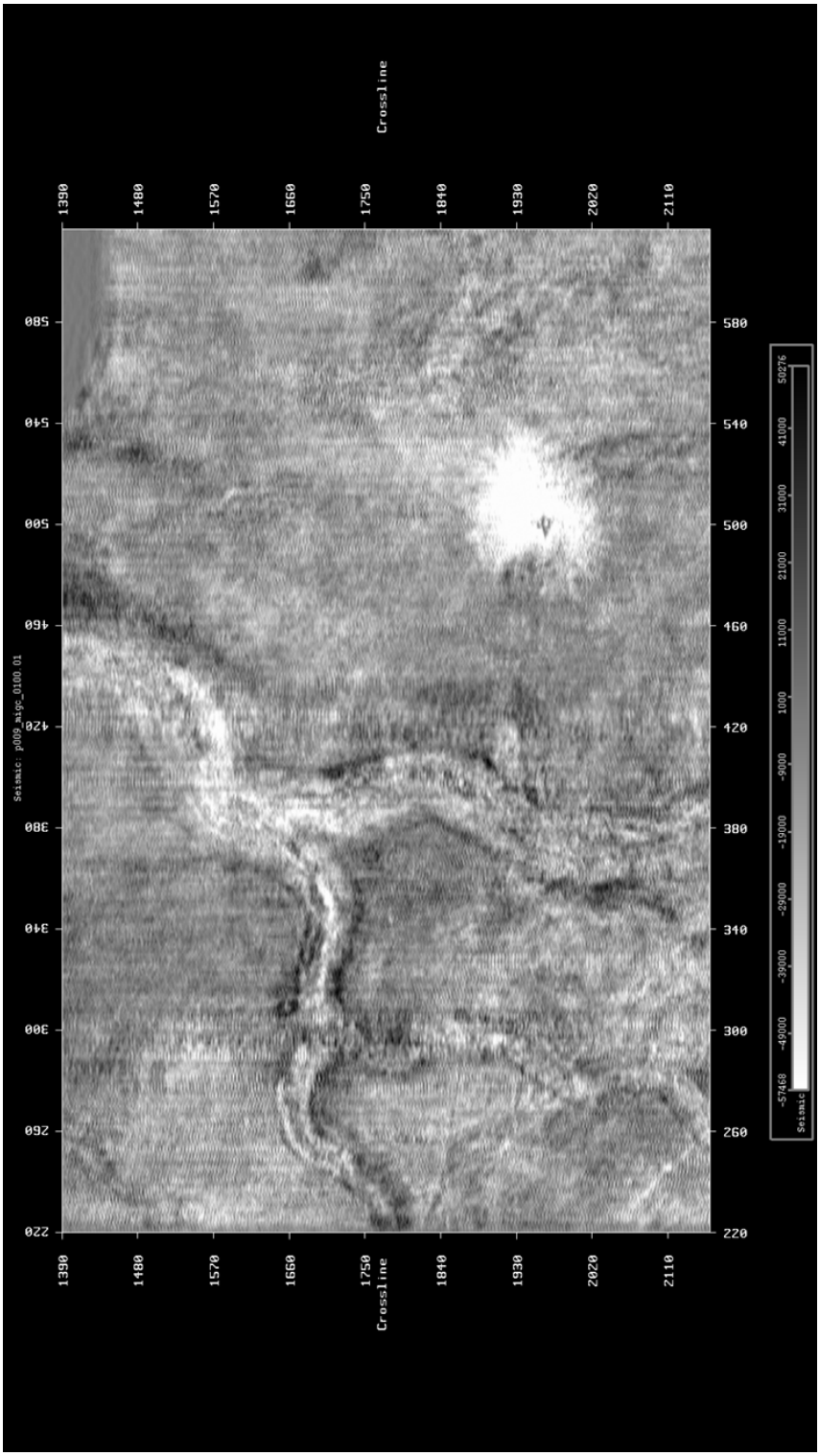

Figure 4.20 – *Migrated cube, offset class 1 - Time slice, 520 ms. Crossline from 1390-2160. Subline from 220-617.*

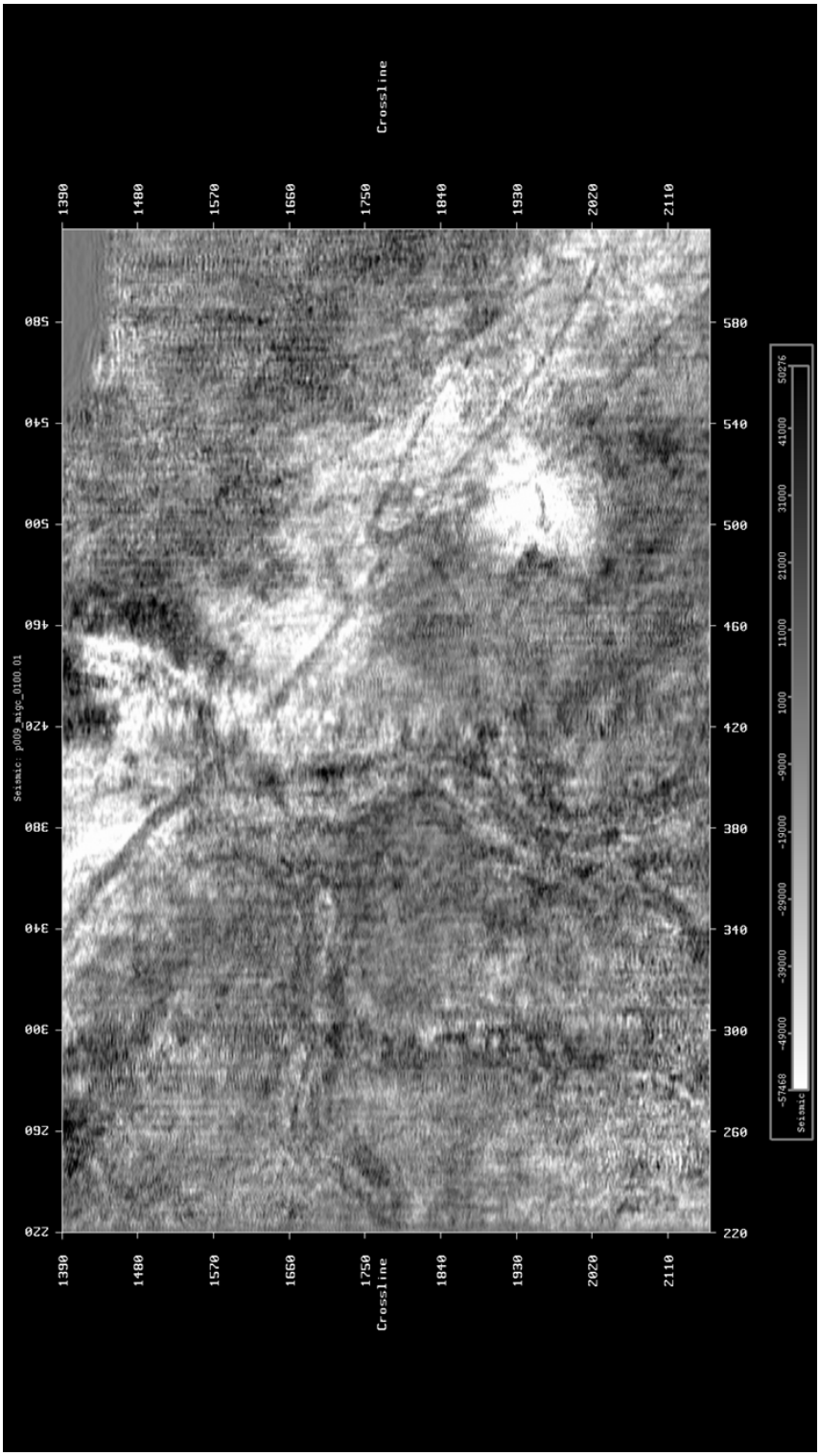

Figure 4.21 – *Migrated cube, offset class 1 - Time slice, 650 ms. Crossline from 1390-2160. Subline from 220-617.*

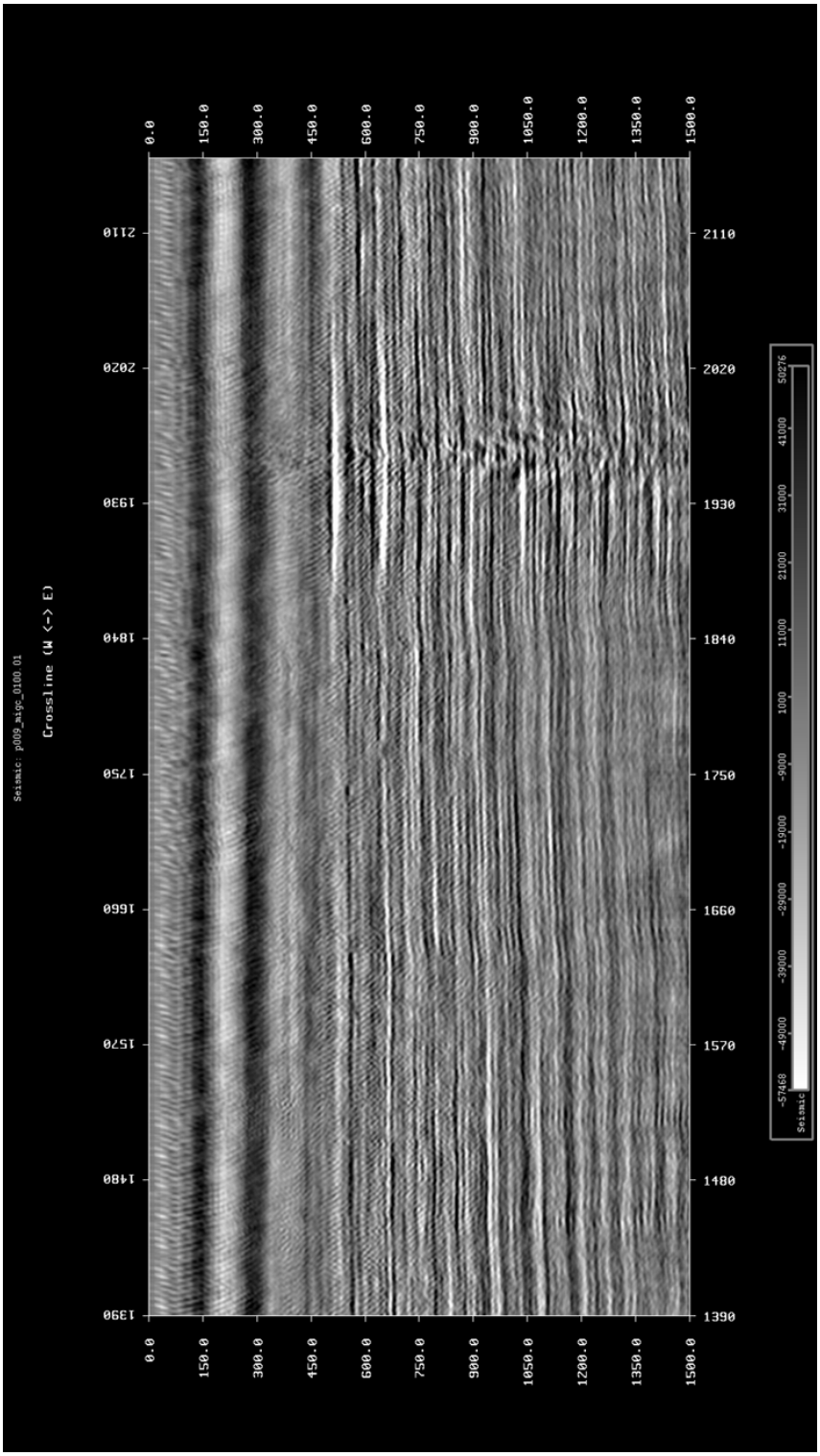

Figure 4.22 – *Migrated cube, offset class 1 - Subline by well. Two-way traveltime in ms from 0-1500, crossline from 1390-2160.*

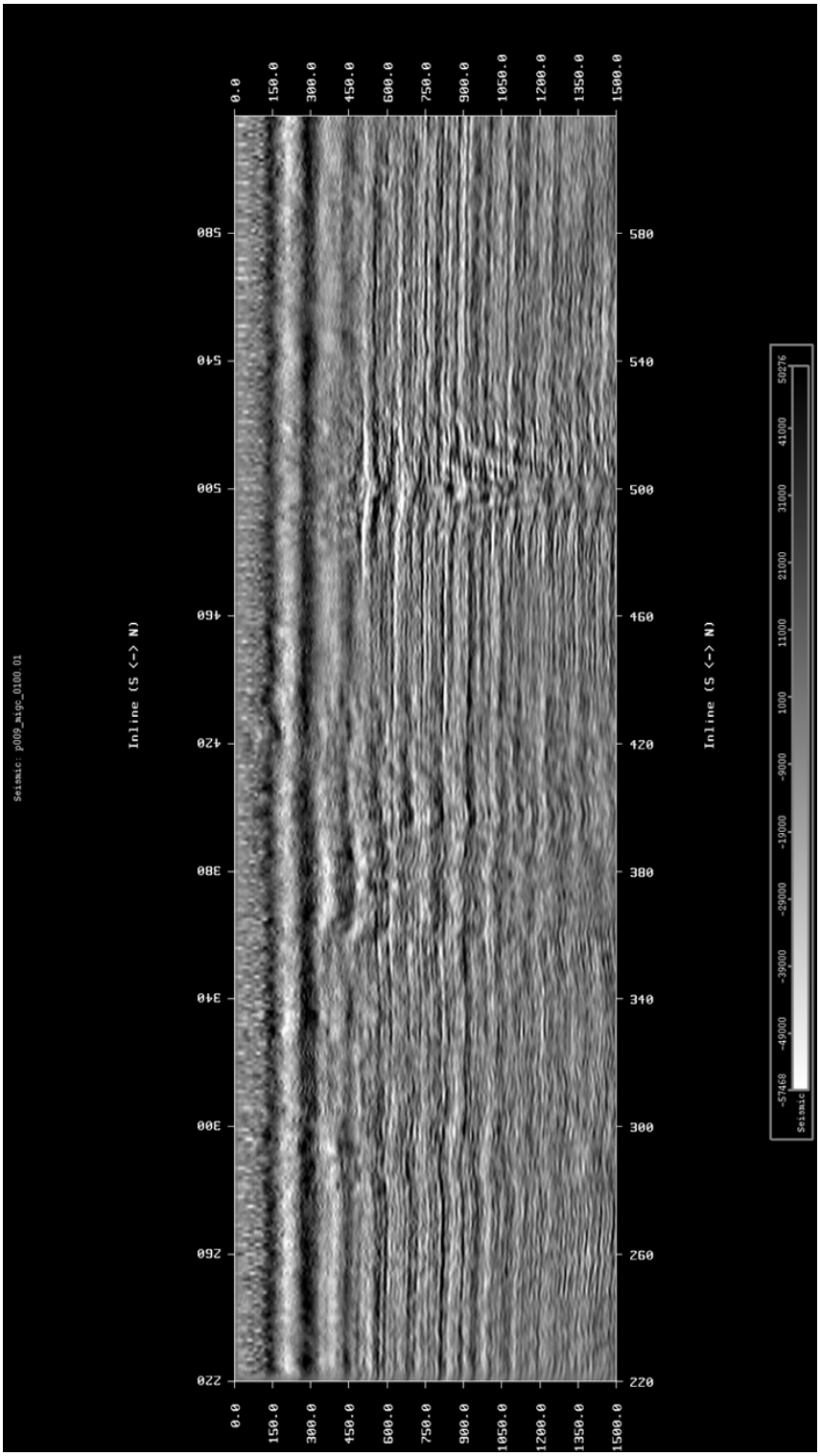

Figure 4.23 – *Migrated cube, offset class 1 - Crossline by well. Two-way traveltime in ms from 0-1500. Subline from 220-617.*

Chapter 5

Discussion

Geohazards must be recognized in the modern offshore hydrocarbon exploration and production. By actively assessing the geohazard risk prior to an operation, the industry proactively reduce economical and environmental expenses, and optimize their operational downtime related to accidents and performance anomalies. Interpretation of geohazard data is primarily based on geophysical data input and the resolution of this data is hence the key constraint in the success of the geohazard assessment. Targeted geohazard surveys has therefore traditionally been superior to other shallow hazard investigation solutions due to their high resolution. Broadband technology is now establishing as an industry standard where highly improved acquisition techniques may deliver seismic data up to 150-200 Hz by mitigating the seismic ghosts. The increased resolution compared with conventional seismic now suggest broadband acquired data to be a reasonable alternative to geohazard surveys in the risk assessment.

As of second fiscal quarter of 2015, oil price is down approximately 40 % compared to second fiscal quarter of 2014. The 12th of December 2014, oil price reached 52.32 USD/bbl, an all time low since 2009, due to a severe shake-up in the global market balance. Introduction of unconventional US hydrocarbon production limited the American import of oil, creating a global oversupply, sending benchmark commodity Brent Crude oil price down from $>$ 110 USD/bbl to $\pm$ 60 USD/bbl in less then six months. Oil companies are collectively responding by cutting costs to reduce operational expenses and maintain the dividends to shareholders. This implies an immediate reduction in oil service contracts and -consultancies in the industry, propagating through all of the up- and down-stream value chain. Exploration campaigns are postponed, rigs are taken out of market, technology investments are reduced, and riskier projects are abandoned in favor of a predictable business-as-usual strategy. Overall, the investments in projects and technology are greatly reduced, and the oil companies are looking for affordable ways to maintain safe operations in the reduced oil price environment.

Both broadband surveys and geohazard surveys are expensive, requiring extra acquisition effort, and hence comes at an great cost for the oil companies on a tight budget.

However, reduction in investments can not come on the expense of safety and environmental concerns, and geohazard assessments are consequently carried out according to regulations and law, regardless of demanding market conditions. Broadband processing of conventional data may hence appear as a cost effective solution to the geophysical data input of the geohazard assessment. By broadband processing data acquired previously in the exploration or production campaign, processing contractors may deliver high resolution data input to the geohazard studies at a reduced cost compared to broadband surveys and geohazard surveys. By targeting the most typical shallow geohazard scenarios and strictly focusing on deghosting and strengthening of signal-to-noise ratio, the output seismic cube may be a qualified substitute for other expensive solutions.

As shown in the North Sea Case study the workflow imaged the targeted shallow gas hazard, and defined the extent and magnitude of the recipients using the described approach. In an industry scenario this would provide excellent data foundation input to a geohazard analysis. The processing enhance the shallow gas by effectively targeting deghosting, denoising and demultiple in a fast track inspired workflow. Additionally the work provide valuable insights on working with data acquired with different technological standards, more than 20 years ago. As experienced, current processing software and techniques does not always easily implement or support configurations considered outdated in the industry.

Testing the designature parameters introduced challenges. Not only was the exact survey configuration not available as input in the signature modelling software as discussed in Ch. 4.2.1, but the provided survey final report and observers logs claimed different positioning of the guns in the water, a key feature of the signature characteristic. Final report stated 6 meter source depth, while the observers log stated 7 meter source depth. In a typical scenario working with recently acquired data a confirmation of the source depth would have been made quickly, either through contact with contractors or data owners. However, as of 2015 Geco-Prakla does not exists as a sole company, and neither does Saga Petroleum, and for many reprocessing projects similar challenges may rise. The designature testing also illustrates the importance of quality control throughout the workflow, and the ability to predict the outcome of a successful processing step, and it was evident that the algorithm estimation did not work properly. The custom designature, on the other hand, might at first glance appear as a quick fix, but actually handled the signature well. By applying basic geophysical knowledge to shape the signature, the results were significantly better than the algorithm estimated signature. The successful designature source-deghosted data and recovered frequencies in the 80-100 Hz range.

During denoising the linear noise was primary target. Other typical challenges seen in seismic surveys are swell noise, tug noise maybe even seismic interference from other surveys, as discussed in Ch. 2.3, but these were not as pronounced in the data, and therefore not prioritized. The origin of the low frequent linear noise was not obvious, but needed to be assessed nontheless. The K-filter followed by the Radon filter was effective, but could not handle all of the noise, and some residual noise was therefore left. For more advanced processing workflows, further denoise could have been initiated,

for example by sorting into receiver domain where the noise likely would have been arbitrary, hence allowing for filter design in an another transformation domain.

The receiver deghosting algorithm provided by CGG is considered top notch in the industry, and is used actively on client projects. As seen in the results, the ghost is successfully removed from both gathers and stacks, but the clear boost in frequency is not pronounced. With streamer depth at 9 m we should expect the receiver ghost notch at $\pm$ 83 Hz in the data. The deghosting algorithm should hence flatten the spectrum and account for the ghost notch at this frequency, even potentially boosting noise around the ghost notch. The lack of frequency enhancement might very well be due to natural notch diversity in the acquisition stage. In earlier seismic acquisition streamer depth control was less precise than today, potentially allowing for variations in streamer depth, creating for a broader range of ghost notches in the frequency spectrum then what the linear Radon operator was able to account for.

The tau-p gap deconvolution operator proved very effective for multiple modelling at the shallow depths. The autocorrelation filter produced a realistic noise model, and handled most of the water-layer multiples in the data. It also preserved the frequency spectrum and additionally targeted most of the residual linear noise, most likely during inverse transformation back from tau-p domain. Most literature on broadband processing of conventional data puts emphasis on deep water surveys. This is due to their more convenient multiple period accounting for a pronounced move-out making all demultiple algorithms easier. However the simple geological structures and and shallow target in the North Sea case study provided a stable platform for the tau-p gap deconvolution demultiple operator. If the tau-p gap deconvolution had not managed the multiples sufficiently, a two-dimensional surface related multiple elimination algorithm would be implemented, requiring more testing and computational power.

The migration successfully handled the diffraction hyperbolas, outputting the seismic cube in its final form. The Kirchhoff migration requires large computational power, and the processing run needed to be booked in advance on supercomputer clusters in UK. This limited the possibilities of parameter testing, but the algorithm provided great results for all offset classes, although main emphasis was put on first offset class. The seismic cube are far from perfect and suffers badly from an unknown acquisition footprint in the upper 450 ms. The sea-bottom is also ruined, likely due to the same reason. The gas target however, is below this acquisition footprint, and display clear amplitude anomalies on both time slices and in cross- and subline stacks. The extent and magnitude of the gas migration is clear, potentially providing a very useful input for a geohazard assessment scenario in an industry case study.

Chapter 6

Conclusion

The work has displayed that conventional 3D exploration seismic data can be utilized for a shallow gas geohazard study through targeted processing. The workflow specifically focused on challenges related to fundamental noise and ghosts, and was able to image two gas recipients at shallow depths. We were able to define the extents and magnitudes of the gas hazards, and provide a foundation for further studies in the area. A few key conclusions for the processing workflow can be stated:

- Broadband processed conventional 3D exploration seismic may serve as a valuable data input substitute for site survey data in a geohazard study.
- Processing and reprocessing old vintage data might offer unforeseen challenges, especially related to modern software algorithms performance with outdated technological standards and acquisition conventions parameter input.
- The tau-p gap deconvolution is an effective demultiple operator for targets in shallow, flat structures.
- Hi-end deghosting operators may not run ideally on old vintage data due to natural notch diversity in acquisition stage resulting from subpar depth control of seismic streamers.

Chapter 7

Recommendations

Due to the time constraints of this study, some steps were not given sufficient attention from a professional seismic contractor point of view. More time could have been spent on each processing steps, using further parameter testing to enhance the frequency spectrum and targets. In addition, the sea-bottom and target overburden was clearly not imaged correctly. However the provided workflow serves as a foundation for future work on this North Sea case study. From the author's point of view, further work on this case should be focused towards three main studies:

- Solve the acquisition footprint challenge on the sea-bottom and in target overburden.
- Compare broadband processed 3D exploration data with available site survey over same area in a geohazard study, focusing on resolution and quantitative interpretation.
- Create a 4D co-processing sequence with the proposed workflow outline, using the 1991 data set and 2005 the QUAD 30 phase V / NQ8, CGG Multiclient survey to express a time-lapse response, imaging the migration of the gas over the time interval.

References

Amundsen, L., and M. Landrø, 2010a: Marine Seismic Sources Part I. *GEO ExPro*, **7** (1), 32–35.

Amundsen, L., and M. Landrø, 2010b: Marine Seismic Sources Part II. *GEO ExPro*, **7** (1), 68–72.

Amundsen, L., and M. Landrø, 2011: Marine Seismic Sources Part VI: High Frequency Signals From Air-Guns. *GEO ExPro*, **8** (a), 68–74.

Amundsen, L., and M. Landrø, 2013a: Broadband seismic technology and beyond, part i. *GEO ExPRO*, **10** (1), 78–82.

Amundsen, L., and M. Landrø, 2013b: Broadband seismic technology and beyond, part ii: Exorcizing seismic ghosts. *GEO ExPRO*, **10** (2), 88–91.

Amundsen, L., H. Zhou, A. Reitan, and A. B. Weglein, 2013: On seismic deghosting by spatial deconvolution. *Geophysics*, **78** (6), V267–V271, dx.doi.org/10.1190/GEO2013-0198.1.

Avseth, P., T. Mukerji, and G. Mavko, 2005: *Quantitative Seismic Interpretation*. 1st ed., Cambridge University Press.

Beasley, C. J., R. Coates, Y. Ji, and J. Perdomo, 2013: Wave equation receiver deghosting: a provocative example. *SEG Expanded Abstract*, 4226–4230.

Brothers, L. L., J. T. Kelly, M. L. Maynard, D. F. Belknap, and S. M. Dickson, 2010: Development in the Gulf of Maine: Avoiding Geohazards and Embracing Opportunities. *Maine Policy Review*, **19**(1), 46–57, http://digitalcommons.library.umaine.edu/mpr/vol19/iss1/7/.

Bunting, T., P. Watterson, and M. Vassallo, 2013: IsoMetrix; Isometrically sampled towed-streamer marine seismic data. *Thirteenth International Congress of the Brazilian Geophysical Society Expanded Abstracts*, 1177–1180.

Campbell, K. J., 1999: Deepwater Geohazards: How significant are they? *Leading Edge*.

Campbell, K. J., 2003: Marine Engineering Geophysics: Meeting the Deepwater Geo-

hazards Challenge. *SEG Expanded Abstract*, 1241–1252, http://dx.doi.org/10.4133/1.2923129.

Carlson, D., A. Long, W. Söllner, H. Tabti, R. Tenghamn, and N. Lunde, 2007: Increased resolution and penetration from a towed dual-sensor streamer. *First Break*, **25** (12), 71–77.

Chopra, S., and K. J. Marfurt, 2007: *Seismic Attributes for Prospect Identification and Reservoir Characterization*. No. 11 ed., Society of Exploration Geophysicists.

Davis, A. M., 1992: Shallow gas: an overview. *Continental Shelf Research*, **12** (10), 10771079, http://dx.doi.org/10.1016/0278-4343(92)90069-V.

Dutta, N. C., R. W. Utech, and D. Shelander, 2010: Role of 3D seismic for quantiative shallow hazard assessment in deepwater sediments. *The Leading Edge*, **29** (8), 930–942, http://dx.doi.org/10.1190/1.3480006.

Ebuna, D. R., T. J. Mitchell, P. J. Hogan, S. Nishenko, and G. H. Greene, 2013: High-resolution offshore 3D seismic geophysical studies of infrastructure geohazards. *SAGEEP Expanded Abstract*.

Elboth, T., and D. Hermansen, 2009: Attenuation of noise in marine seismic data. *SEG TEchnical Program Expanded Abstracts 2009*, 3312–3316, http://dx.doi.org/10.1190/1.3255547.

Farouki, M., F. Paone, A. Marceglia, F. Felappi, and C. Monti, 2012: Utilizing short offset data from a 3D exploration survey for regional seabed morphology and geohazard mapping in Makassar straits, Indonesia. *SEG Expanded Abstract*, 1–5, http://dx.doi.org/10.1190/segam2012-0891.1.

Farouki, M., and S. Sakamoto, 2013: Utilizing 3D exploration seismic data for seabed mapping and near surface geohazard investigation. *SEGJ Expanded Abstract*, 273–276, http://dx.doi.org/10.1190/segj112013-069.

Haavik, K. E., and M. Landrø, 2014: Iceberg ploughmarks illuminated by shallow gas in the central North Sea. *Quaternary Science Reviews*, **103** (1), 3450, http://dx.doi.org/10.1016/j.quascirev.2014.09.002.

Hammond, J. W., 1962: Ghost elimination from reflection records. *Geophysics*, **27** (1), 48–60, http://dx.doi.org/10.1190/1.1438977.

Hesthammer, J., M. Landrø, and H. Fossen, 2001: Use and abuse of seismic data in reservoir characterisation. *Marine and Petroleum Geology*, **18**, 635–655.

ISO17776:2000, 2000: *International standard. Petroleum and natural gas industries - Offshore production installations Guidelines on tools and techniques for hazard identification and risk assessment.* International organization for standardization ed., ISO 17776:2000.

Judd, A., and M. Hovland, 2009: *Seabed Fluid Flow: The Impact on Geology, Biology and the Marine Environment*. 1st ed., Cambridge University Press.

Kallweit, R. S., and L. C. Wood, 1982: The limits of resolution of zero-phase wavelets. *Geophysics*, **47** (7), 1035–1046, http://dx.doi.org/10.1190/1.1441367.

Kroode, F. t., S. Bergler, C. Corsten, J. W. de Maag, F. Strijbos, and H. Tijhof, 2013: Broadband seismic data - The importance of low frequencies. *Geophysics*, **78** (2), http://dx.doi.org/10.1190/geo2012-0294.1.

Landrø, M., 2011: Seismic monitoring of an old underground blowout - 20 years later. *First Break*, **6**, 39–48, http://dx.doi.org/10.3997/1365-2397.2011017.

Leet, L. D., 1937: A plutonic phase in seismic prospecting. *Bulletin of the Seismological Society of America*, **27** (2), 97–98.

Lindsey, J. P., 1960: Elimination of seismic ghost reflections by means of a linear filter. *Geophysics*, **25** (1), 130–140, http://dx.doi.org/10.1190/1.1438679.

Mallicks, S., and N. C. Dutta, 2002: Shallow water flow prediction using prestack waveform inversion of conventional 3D seismic data and rock modeling. *The Leading Edge*, **21** (7), 675–680, http://dx.doi.org/10.1190/1.1497323.

Meunier, J., 2011: *2011 Distinguished Instructor Short Course: Seismic Acquisition from Yesterday to Tomorrow*. Distinguished instructor series, no. 14 ed., Society of Exploration Geophysicist.

NGI, 2005: Offshore Geohazards - Summary Report. *Research institution-based strategic project 2002-2005*, 1.

Opseth, T. L., B. T. Tibesen, B. Syrstad, A. Huse, L. Bolstad, and A. Saasen, 2009: Curing Shallow Water Flow in a North Sea Exploration Well Exposed to Shallow Gas. *Society of Petroleum Engineers*, Offshore Europe, 8–11 September, Aberdeen, UK, http://dx.doi.org/10.2118/124607-MS.

Özbek, A., A. K. Özdemir, D.-J. v. Manen, and K. Eggenberger, 2010: Crossline wavefield reconstruction from multicomponent streamer data: joint interpolation and 3D up/down separation by generalized matching pursuit. *SEG Expanded Abstract*, 3599–3603, http://dx.doi.org/10.1190/1.3513598.

Özdemir, A. K., P. Caprioli, A. Özbek, E. Kragh, and J. O. A. Robertsson, 2008: Optimized deghosting of over/under towed-streamer data in the presence of noise. *The Leading Edge*, **27**, 190–199, http://dx.doi.org/10.1190/1.2840366.

Plets, R., J. Dix, and R. Bates, 2013: *Marine Geophysics Data Acquisition, Processing and Interpretation*. 1st ed., Historic England.

Poole, G., 2013: Pre-migration receiver de-ghosting and re-datuming for variable depth streamer data. *SEG Technical Program Expanded Abstracts*, 4216–4220, http://dx.doi.org/10.1190/segam2013-0541.1.

Ray, C. H., and N. A. Moore, 1982: High resolution, marine seismic stratigraphic system. *U.S Patent no 4,353,121.*

Remen, A., 1991: Flow paths and shallow gas migration. *The 2/4-14 Experience Transfer Seminar*, (Stavanger), 16–17. January.

Robertsson, J. O. A., and L. Amundsen, 2014: Wave equation processing using finite-difference propagators, Part 2: Deghosting of marine hydrophone seismic data. *Geophysics*, **79** (6), T301–T312, dx.doi.org/10.1190/GEO2014-0152.1.

Robinson, E. A., and S. Treitel, 2000: *Geophysical Signal Analysis.* Society of Exploration Geophysicists.

Sharp, A., and G. Badalini, 2013: Using 3D seismic data to map shallow-marine geohazards: a case study from the Santos Basin, Brazil. *Petroleum Geoscience*, **19** (2), 157–167, http://dx.doi.org/10.1144/petgeo2011-063.

Sheriff, R. E., 2002: *Encyclopedic dictionary of applied geophysics.* 4th ed., Society of Exploration Geophysicists.

Sheriff, R. E., and L. Geldart, 1995: *Exploration Seismology.* 2nd ed., Cambridge University Press.

Sills, G. C., and S. J. Wheeler, 1992: The significance of gas for offshore operations. *Continental Shelf Research*, **12** (10), 12391250, http://dx.doi.org/10.1016/0278-4343(92)90083-V.

Simm, R., and R. White, 2002: Phase, polarity and the interpreter's wavelet. *First Break*, **20** (5), 277–281, http://onlinelibrary.wiley.com/doi/10.1046/j.1365-2397.2002.00277.x/abstract.

Solheim, A., R. Bhasin, and F. V. Deblasio, 2005: International Centre For Geohazards: Assessment, prevention and mitigation of geohazards. *Norwegian Journal Of Geology*, **ICG**, 45–62.

Sønneland, L., 1986: 2D deghosting using vertical receiver arrays. *SEG Expanded Abstract.*

Sønneland, L., L. E. Berg, P. Eidsvig, A. Haugen, B. Fotland, and J. Vestby, 1986: 2-D deghosting using vertical receiver arrays. *SEG Expanded Abstract*, 516–519, http://dx.doi.org/10.1190/1.1893019.

Soubaras, R., 2010: Deghosting by joint deconvolution of a migration and a mirror migration. *SEG Expanded Abstract*, 3406–3410.

Soubaras, R., and Y. Lafet, 2011: Variable-depth streamer acquisition: Broadband data for imaging and inversion. *Geophysics*, **78** (2), WA27–WA39, http://dx.doi.org/10.1190/geo2012-0297.1.

Szabó, T., 2001: Drilling through shallow gas zones in Hungary. *Oil And Gas Business Journal*, **2**.

Tenghamn, R., S. Vaage, and C. Borresen, 2007: A dual-sensor towed marine streamer: Its viable implementation and initital results. *SEG Expanded Abstract*, 989–993, http://dx.doi.org/10.1190/1.2792571.

International Association of Oil & Gas Producers, 2009: *Geohazards from seafloor instability and mass flow*. Report no. 425 ed., OPG.

NORSOK Z-013, 2010: *Z-013 Risk and emergency preparedness assessment*. 3rd ed., Standard Norge.

Oil & Gas Journal, 2007: Global Offshore Oil - 1: Exploration trends show continued promise in world's offshore basins. *Oil & Gas Journal*, **105** (9), authors: Sandrea, I. and Sandrea, R.

Toxopeus, G., R. van Borselen, R. H. Baardman, and E. Ødegaard, 2011: Advanced Geohazard Assessment in Shallow Water through the Estimation of Primaries by Sparse Inversion. *SEG Expanded Abstract*, 3526–3530, http://dx.doi.org/10.1190/1.3627932.

Wang, P., and C. Peng, 2012: Premigration deghosting for marine towed streamer data using a bootstrap approach. *SEG Expanded Abstract*, 1–5, http://dx.doi.org/10.1190/segam2012-1146.1.

Weimer, P., and C. Shipp, 2004: Mass Transport Complex: Musing on Past Uses and Suggestions for Future Directions. *Offshore Technology Conference*, 1–10, http://dx.doi.org/10.4043/16752-MS.

Yilmaz, Ö., 2001: *Seismic Data Analysis: Processing, and Interpretation of Seismic Data*. 2nd ed., Electronic Edition Published in 2008.

Zhou, Z., M. Cvetkovic, B. Xu, and P. Fontana, 2012: Analysis of a broadband processing technology applicable to conventional streamer data. *First Break*, **30** (10), 77–82.

Zoeppritz, K., 1919: On the reflection and transmissions of seismic waves at surfaces of discontinuity. *Classics Of Elastic Wave Theory, SEG Geophysics Reprint Series*, **24**, 363–376, translated by Henning Hoeber in 2007 from the original German text, published in *Nachrichten von der Gesellschaft der Wissenschaften zu Gttingen - Mathematisch-Physikalische Klasse*, http://dx.doi.org/10.1190/1.9781560801931.ch3n.